AD-A089 306 AIR FORCE ROCKET PROPULSION LAB EDWARDS AFB CA F/G 21/8.2
STABILITY PREDICTION FOR SOLID PROPELLANT ROCKET MOTORS WITH HI--ETC(U)
AUG 80 G A FLANDRO
UNCLASSIFIED AFRPL-TR-79-98 NL

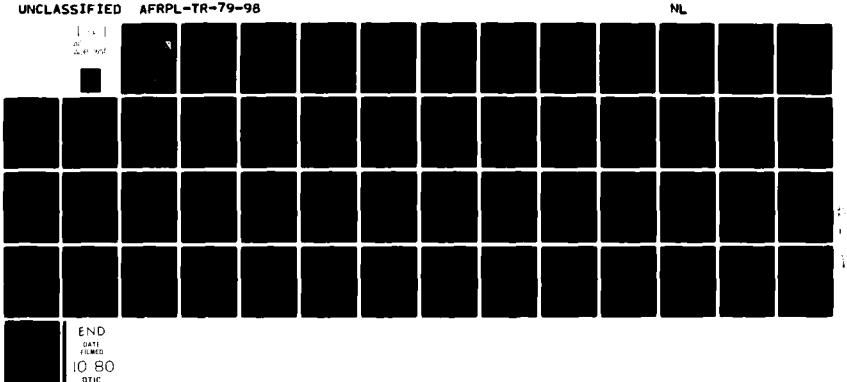

END
DATE FILMED
10 80
DTIC

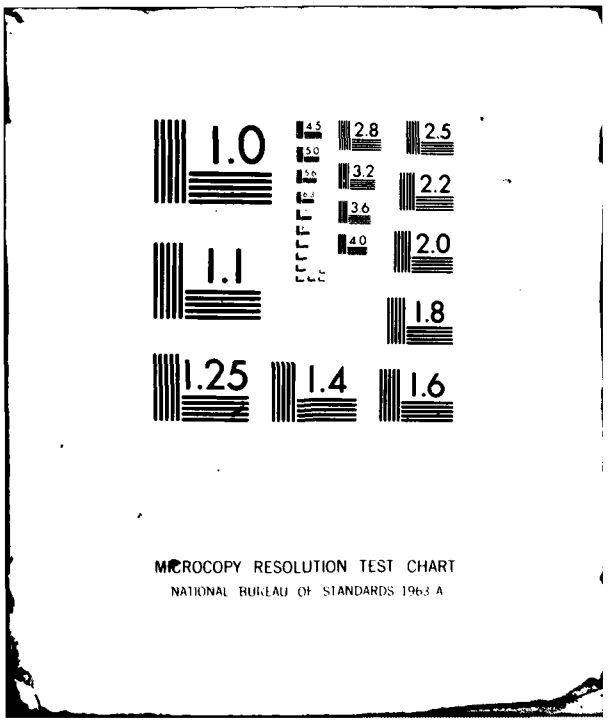
1.0
1.1
1.25
1.4
1.6
1.8
2.0
2.2
2.5
2.8
3.2
3.6
4.0
4.5
5.0
MICROCOPY RESOLUTION TEST CHART
NATIONAL BUREAU OF STANDARDS 1963 A

LEVEL II

AFRPL-TR-79-98

# STABILITY PREDICTION FOR SOLID PROPELLANT ROCKET MOTORS WITH HIGH-SPEED MEAN FLOW

AIR FORCE ROCKET PROPULSION LABORATORY
EDWARDS AFB CA 93523

Author: Gary A. Flandro (University of Utah)



August 1980

FINAL REPORT

*Approved for Public Release*
*Distribution Unlimited*

Air Force Rocket Propulsion Laboratory
Director of Science and Technology
Air Force Systems Command
Edwards AFB, California 93523

## NOTICES

When U.S. Government drawings, specifications, or other data are used for any purpose other than a definitely related government procurement operation, the Government thereby incurs no responsibility nor any obligation whatsoever, and the fact that the Government may have formulated, furnished, or in any way supplied the said drawings, specifications, or other data is not to be regarded by implication or otherwise, or in any manner, licensing the holder or any other person or corporation, or conveying any rights or permission to manufacture, use, or sell any patented invention that may in any way be related thereto.

## FOREWORD

This report was prepared by the author while he was working as a visiting Professor in the Combustion Section (PACC) of the Propulsion Analysis Division (PA), of the Air Force Rocket Propulsion Laboratory, Edwards AFB, CA. This report documents an investigation conducted during the time period June through September, 1978, as part of the program entitled "In-House Combustion Analysis" (JON: 573010CM). The technical program manager for this program was Mr Jay N. Levine.

This report has been reviewed by the Information Office/TSPR and is releasable to the National Technical Information Service (NTIS). At NTIS it will be available to the general public, including foreign nations. This technical report has been reviewed and is approved for publication; it is unclassified and suitable for general public release.

JAY N. LEVINE
Project Manager

WILBUR C. ANDREPONT
Chief, Combustion Technology Branch

FOR THE COMMANDER

EUGENE G. HABERMAN
Chief, Propulsion Analysis Division

UNCLASSIFIED

SECURITY CLASSIFICATION OF THIS PAGE (When Data Entered)

| REPORT DOCUMENTATION PAGE | READ INSTRUCTIONS BEFORE COMPLETING FORM |
|---|---|
| 1. REPORT NUMBER: AFRPL-TR-79-98 | 2. GOVT ACCESSION NO.: AD-A089306 |
| 3. RECIPIENT'S CATALOG NUMBER | |
| 4. TITLE (and Subtitle): STABILITY PREDICTION FOR SOLID PROPELLANT ROCKET MOTORS WITH HIGH SPEED MEAN FLOW. | 5. TYPE OF REPORT & PERIOD COVERED: FINAL REPORT, |
| | 6. PERFORMING ORG. REPORT NUMBER |
| 7. AUTHOR(s): Gary A. Flandro (University of Utah) | 8. CONTRACT OR GRANT NUMBER(s) |
| 9. PERFORMING ORGANIZATION NAME AND ADDRESS: Air Force Rocket Propulsion Laboratory/PACC, Edwards Air Force Base, CA 93523 | 10. PROGRAM ELEMENT, PROJECT, TASK AREA & WORK UNIT NUMBERS: JON 5730[illegible]OVA |
| 11. CONTROLLING OFFICE NAME AND ADDRESS | 12. REPORT DATE: August 1980 |
| | 13. NUMBER OF PAGES: 60 |
| 14. MONITORING AGENCY NAME & ADDRESS (if different from Controlling Office) | 15. SECURITY CLASS. (of this report): UNCLASSIFIED |
| | 15a. DECLASSIFICATION/DOWNGRADING SCHEDULE: NA |

16. DISTRIBUTION STATEMENT (of this Report)

Approved for public release; distribution unlimited.

17. DISTRIBUTION STATEMENT (of the abstract entered in Block 20, if different from Report)

18. SUPPLEMENTARY NOTES

19. KEY WORDS (Continue on reverse side if necessary and identify by block number)

Combustion Instability
Motor Instability
Solid Rocket Motors
Acoustics

20. ABSTRACT (Continue on reverse side if necessary and identify by block number)

Current stability prediction calculations for solid propellant rocket motors are based upon a simple first-order perturbation solution which assumes an incompressible chamber mean flow. Since combustion instability is frequently observed in motors with large length-to-diameter and low port-to-throat area ratios, there is concern that the standard stability techniques should be extended to apply to cases where high-speed mean flows are present. This report shows how the basic stability analysis can be extended by carrying

DD FORM 1 JAN 73 1473 EDITION OF 1 NOV 65 IS OBSOLETE

UNCLASSIFIED

SECURITY CLASSIFICATION OF THIS PAGE (When Data Entered)

307720

additional terms in the perturbation expansions. Compressibility affects the calculations in several ways. The acoustic mode shapes predicted in the linear model are distorted and the mean thermodynamic properties may vary significantly from point to point in the chamber. These variations and distortions alter both the predicted growth rates and also the frequencies for the acoustic modes. Detailed calculations are carried out for a cylindrical grain geometry with longitudinal wave motions. Frequency and growth rate corrections grow quadratically with increases in the port length-to-diameter ratio. Frequency shifts of as much as 30 percent of the linear acoustic frequency predictions may be expected in high L/D motors.

## TABLE OF CONTENTS



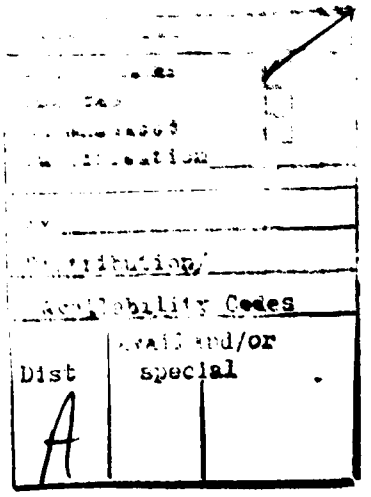

## LIST OF FIGURES

## 1. INTRODUCTION

The current stability prediction calculations for solid propellant rocket motors are based upon a simple first-order perturbation solution of the inviscid equations of motion for the combustion gas flow in the chamber. Thus there is concern over the applicability of the standard stability prediction techniques to cases where high-speed mean flows are present. Such flows are likely to occur in tactical rockets with large length-to-diameter and low port-to-throat area ratios. Nozzleless motors represent an extreme example of this type of design; flow velocities may approach the speed of sound at the grain exit. High-speed flow effects may also be significant in slots and fins and around submerged nozzles especially early in the motor run when burning area is large and flow channel area is small. The purpose of this study is to assess the impact of high-speed mean flow on the stability prediction approach and to generate correction techniques to be applied to existing combustion instability models.

High-speed mean flow affects the stability calculation in several ways. The acoustic wave forms predicted in the linear model are distorted and the mean thermodynamic properties such as the speed of sound may vary significantly from point to point in the chamber. These variations may alter both the predicted growth rates and also the frequencies for the acoustic modes. Correct frequency calculations are important since they are crucial in mode identification in an unstable motor.

All acoustic combustion instability models in current use employ a "linearization" of the inviscid equations of motion. This approach was first utilized by McClure (Refs. 1 and 2) and his coworkers and developed more fully by Culick (Refs. 3 and 4). Two Parameters representing respectively the ampli-

---

1. Bird, J. T., McClure, F. T., and Hart, R. W., "Acoustic Instability in the Transverse Modes of Solid Propellant Rockets," 12th International Astronautical Congress, Academic Press, 1963.

2. Cantrell, R. H., and Hart, R. W., "Interaction Between Sound and Flow in Acoustic Cavities: Mass, Momentum, and Energy Considerations," Journal of the Acoustical Society of America, Vol. 36, No. 4, April 1964.

3. Culick, F. E. C., "Acoustic Oscillations in Solid Propellant Rocket Chambers," Astronautica Acta, Vol. 12, No. 2, 1966.

4. Culick, F. E. C., "Interactions Between the Flow Field, Combustion, and Wave Motions in Rocket Motors," NWC-TP-5349, Naval Weapons Center, China Lake, California, June 1972.

tude of the acoustic wave and the mean flow speed are used in expanding the pertinent physical equations describing the gas flow. Combustion effects are represented by admittance boundary conditions at the chamber walls, nozzle entrance and head-end closure. Only linear terms in amplitude and mean flow Mach number are retained and the result is a simple formula for the growth rate which can be evaluated by utilizing linear acoustic mode shapes in integrals taken over the surface and volume of the chamber (Ref. 3). It is clear that this procedure is valid if wave growth at the stability boundary only is required, and if an incompressible, uniform mean flow is present. The assumption of small wave amplitude results in what is called an "initially valid" approximation of the growth process of the waves. Thus the solutions can be considered valid only at the instant growth begins. It may seem unnecessary to emphasize this point since prediction models indeed are based on the stability boundary idea. However, an understanding is crucial if one seeks to improve the linear model by evaluating higher-order terms in the asymptotic expansions. Specifically, the linear model assumes that the small parameters are related by the limit process

$$\lim_{\varepsilon,\, M_b \to 0} (\varepsilon/M_b) = 0 \qquad (1)$$

where $\varepsilon$ is the wave amplitude (proportional to the Mach number of the acoustic velocity) and $M_b$ is the mean flow Mach number at the burning surface. It is readily demonstrated that if one desires to assess the effects of mean flow compressibility and spatial variation of the mean flow field thermodynamic properties then higher-order terms (at least to $O(M_b^2)$) must be retained despite the fact that $M_b$ at the surface is very small.* In order that the expansion process does not lead to spurious results, it is then necessary to modify the limit process given in Equation 1 to the following:

$$\lim_{\varepsilon,\, M_b \to 0} (\varepsilon/M_b^2) = 0 \qquad (2)$$

That is, $\varepsilon = o(M_b^2)$ in the notation of perturbation theory.** In view of

* Mean flow Mach number at the burning surface is typically in the range $0.001 < M_b < 0.01$.

** If this restriction is not made, then it is necessary to evaluate terms of order $\varepsilon^2 M_b$ to produce a valid asymptotic expansion.

the small magnitude of $M_b$, this represents a severe restriction on the amplitude of the wave. The difficulty appears when one attempts to correlate experimental results by use of this theory. By definition, the data represent finite waves, and even the smallest discernable wave motions imply $\varepsilon >> M_b^2$ which violates the fundamental assumption. Limitations of the sort described can only be overcome by either reverting to a completely numerical solution of the problem or by use of a more appropriate perturbation scheme. In regard to the latter approach, it appears that a modification of the two-variable method or method of multiple scales will eventually allow generation of analytical solutions which are valid for a less limited range of values of wave amplitude (Refs. 5 and 6). Such expansions can yield uniformly valid approximations which would be of great utility in understanding the self-limiting characteristics or "limiting amplitude" behavior of solid rocket instability. Such an approach was foregone in the present study, since emphasis was to be on devising computer codes which are now in widespread use. Thus the expansion process implied by Equation 2 forms the basis for the analysis given here. All dynamic and thermodynamic parameters of the mean and oscillating flow fields are expanded in both $\varepsilon$ and $M_b$. Figure 1 will aid the reader in interpreting the degree to which we are attempting to improve the linear theory. Retention of terms of order $(\varepsilon, M_b)$ yields the linear stability model. In what follows, we extend the model to include effects of $O(\varepsilon, M_b^2)$ in order to assess the influence of nonuniform, compressible mean flow and mean chamber thermodynamics. As in the "classical" model, combustion effects and the influence of the nozzle are represented by appropriate admittance boundary conditions. Also, viscosity is assumed to be negligible except insofar as it affects the wave motions near the solid boundaries of the chamber. These influences can be accounted for by corrections to the surface admittance (Ref. 7). However, vorticity generated at the boundary may be convected throughout the flow field and subsequently affect both wave growth and oscillation frequency (Refs. 8 and 9). Since these effects may be especially important in the presence of high mean flow Mach numbers, their influence is retained in

---

5. Cole, J. D., and Kevorkian, J., "Uniformly Valid Asymptotic Approximations for Certain Nonlinear Differential Equations." Nonlinear Differential Equations and Nonlinear Mechanics, Academic Press, 1963.
6. Nayfeh, A. H., Perturbation Methods, Wiley, 1973.
7. Flandro, G. A., "Solid Propellant Admittance Corrections," Journal of Sound and Vibration, Vol. 36, No. 3, 1974.

| Order | $M_b = 0$ | $M_b$ | $M_b^2$ |
|---|---|---|---|
| $\varepsilon$ | Linear acoustics | Linear theory of acoustic combustion instability | Mean flow compressibility effects:<br>waveform distortion<br>frequency shift<br>growth rate effects |
| $\varepsilon^2$ | "Nonlinear" acoustics | Finite wave amplitude effects:<br>waveform distortion<br>steady momentum transport by waves<br>acoustic streaming | Nonlinear interaction between mean flow compressibility and finite wave amplitude effects. |

Figure 1. Expansion of the Equations of Motion.

the formulation. The analysis is carried out for the full three-dimensional geometry with arbitrary shape. The results are applied to longitudinal waves in a high L/D cylindrical grain to demonstrate their potential relevance in the stability prediction problems. It is shown that significant changes in mode frequency and growth rates occur; the corrections grow quadratically with increases in the port length-to-diameter ratio L/D.

8. Culick, F. E. C., "Rotational Axisymmetric Mean Flow and Damping of Acoustic Waves in a Solid Propellant Rocket," AIAA Journal, Vol. 4, No. 8, August 1966.

9. Flandro, G. A., "Rotating Flows in Acoustically Unstable Rocket Motors," PhD Thesis, California Institute of Technology, 1967.

## 2. ANALYSIS

In what follows, the equations of motion, boundary conditions, and assumptions which form the basis for the analysis are first reviewed. The mathematical strategy is then formulated and applied to the problem. Results are given in completely general form. The reader more interested in the applications than the details of the calculation might skip all of this section except the review of the assumptions.

### 2.1. Assumptions

A rigid internally burning propellant grain is assumed.* Only regions of the flow which are subsonic are considered. Influence of the sonic nozzle throat are represented by appropriate admittance functions. Although an inviscid fluid is assumed (no viscous force terms are retained in the momentum equations) the flow is allowed to be rotational; thus a realistic mean flow field is accommodated (Ref. 8) and vorticity generation and transport is represented. The combustion process is assumed to be concentrated at the bounding surface of the chamber and its sensitivity to acoustic fluctuations is represented by an admittance boundary condition as in the linear stability analysis. The effect of regression of the burning surface as propellant is consumed is neglected since the associated characteristic time is long compared to the period typical of the gas oscillations and amplification time for the waves. The gas is assumed thermodynamically perfect.

### 2.2. Equations of Motion

The motion of a compressible inviscid gas is governed by

$$\frac{\partial \rho}{\partial t} + \nabla \cdot (\rho \underline{u}) = 0 \tag{3}$$

---

* Some effects of rigid body motion of the combustion chamber on structure and growth of acoustic waves are assessed in Reference 9.

$$\rho \frac{D\underline{u}}{Dt} + \frac{\nabla P}{\gamma} = o \tag{4}$$

$$\rho \frac{DT}{Dt} - \left(\frac{\gamma-1}{\gamma}\right) \frac{DP}{Dt} = o \tag{5}$$

$$P = \rho T \tag{6}$$

The equations are written in terms of the dimensionless variables:

$$P = P'/Po$$

$$\rho = \rho'/\rho o$$

$$\underline{u} = \underline{u}'/a_o$$

$$T = T'/To$$

$$\underline{r} = \underline{r}'/R$$

$$t = (a_o/R)t'$$

where R is a characteristic chamber radius and $a_o$ is the stagnation speed of sound in the chamber. Dimensional quantities are denoted by primes and subscript *o* indicates the stagnation values of the principal thermodynamic variables (dimensional) in the absence of wave motion.

## 2.3. Perturbation Expansions

In order to extend the linear theory it is necessary to utilize double perturbation series of the principal variables in terms of the two fundamental scaling parameters $M_b$ and $\varepsilon$. $M_b$ is the mean flow Mach number at the burning

$$P^{(o)} = 1 + M_b^2 \; P + 0\,(M_b^4) \tag{10}$$

$$P^{(1)} = P^{(10)} + M_b P^{(11)} + 0\,(M_b^2)$$

$$\underline{u}^{(1)} = \underline{u}^{(10)} + M_b \underline{u}^{(11)} + 0\,(M_b^2)$$

$P$ reflects the effects of compressibility on the steady pressure distribution in the cavity. $P$ and $\underline{U}$ are usually determined as functions of position in the chamber as part of the motor internal ballistics design process. For complicated geometries they cannot be described in terms of simple mathematical functions, but can be handled numerically in the calculations.

## 2.4. Boundary Conditions

Since the combustion process takes place in a thin lamina of fluid at the wall of the chamber, it is possible to represent the effects of combustion as a boundary condition on the flow at the interface. This is accomplished by introducing the admittance function A such that

$$\hat{n} \cdot \tilde{\underline{u}} = -M_b \left(\frac{\tilde{P}}{\gamma}\right) A \tag{11}$$

at the boundary. $\tilde{\underline{u}}$ and $\tilde{P}$ are the (complex) velocity and pressure fluctuations at the wall. $\hat{n}$ is an outward pointing unit vector normal to the chamber wall, and $\gamma$ the ratio of specific heats is inserted for convenience. This notation for A is the same as originally employed by Culick (Ref. 3). In later work he altered this definition somewhat by defining $\hat{n}$ to be an <u>inward</u> pointing normal unit vector and by omitting the scaling factor $M_b$ from the definition. To distinguish the two definitions, we put

$$A = \frac{A_b}{M_b} \tag{12}$$

where $A_b$ is the admittance function normally used in the literature (Refs. 4 and 10). The use of the older notation is adhered to in this analysis since higher-order expansions in $M_b$ are evaluated--carrying superfluous $M_b$'s in the already sufficiently complicated algebraic expressions is clearly not a sensible procedure. It is well-known that the algebra involved in perturbation expansions increases enormously as higher order terms are retained; it is thus essential to use efficient notation. An additional advantage of the present notation is that numerical values of $|A|$ are in the range $-10<|A|<10$ such that very tiny numbers and resulting additional possibility of error does not affect the calculations. Note that A is a complex number:

$$A = A^{(r)} + i\, A^{(i)} \tag{13}$$

It will be shown that knowledge of both real and imaginary parts is necessary in the proper evaluation of high-speed mean flow effects.

2.5. Derivation of Wave Equation

Equations (3) through (6) may be recombined to yield the set

$$\frac{\partial P}{\partial t} + \gamma P \nabla \cdot \underline{u} = \underline{u} \cdot \nabla P \tag{14}$$

$$\rho \frac{D\underline{u}}{Dt} + \frac{\nabla P}{\gamma} = 0 \tag{15}$$

Utilizing expansions (9) and (10) one finds to $0(\varepsilon)$ (retaining terms to $0\ (M_b{}^2)$),

$$\frac{\partial p^{(1)}}{\partial t} + \gamma \nabla \cdot \underline{u}^{(1)} = -M_b\ [\underline{U} \cdot \nabla p^{(1)}] - M_b{}^2\ [\underline{u}^{(1)} \cdot \nabla p + \gamma p \nabla \cdot \underline{u}^{(1)}] \tag{16}$$

---

10. Anonymous, T-BURNER MANUAL, CPIA Publication No. 191, November 1969.

$$\frac{\partial \underline{u}^{(1)}}{\partial t} + \frac{\nabla p^{(1)}}{\gamma} = -M_b \left[\nabla \underline{U} \cdot \underline{u}^{(1)} - \underline{u}^{(1)} \times \zeta\right] + \frac{M_b^2}{\gamma}\left[\frac{\bar{p}\nabla p^{(1)}}{\gamma} + \rho^{(1)}\nabla \bar{p}\right] \tag{17}$$

where $\zeta = \nabla \times \underline{U}$ is the mean flow vorticity.

The wave equation governing the acoustic pressure fluctuations is derived by subtracting the divergence of the momentum equation (17) from the time derivative of the continuity equation (16):

$$\frac{\partial^2 p^{(1)}}{\partial t^2} - \nabla^2 p^{(1)} = M_b \left[-\frac{\partial}{\partial t}\left(\underline{U}\cdot\nabla p^{(1)}\right) + \gamma\nabla\cdot\nabla\left(\underline{U}\cdot\underline{u}^{(1)}\right) - \gamma\nabla\cdot\left(\underline{u}^{(1)} \times \zeta\right)\right] - M_b^2\left[\frac{\partial}{\partial t}\left(\underline{u}^{(1)}\cdot\nabla\bar{p} + \gamma\bar{p}\nabla\cdot\underline{u}^{(1)}\right) + \nabla\cdot\left(\frac{\bar{p}\nabla p^{(1)}}{\gamma} + \rho^{(1)}\nabla\bar{p}\right)\right] \tag{18}$$

Again, terms of order $M_b^2$ are retained to correctly represent the influence of the high-speed compressible mean flow. It is important to note that this implies that all $O(M_b^2)$ corrections (e.g. $P^{(11)}$, $\underline{u}^{(11)}$, etc.) must eventually be calculated to properly evaluate the wave equation. In anticipation of oscillations, it is appropriate to assume that all dependent variables exhibit exponential time dependence:

$$p^{(1)} = \gamma p^{(1)} e^{iKt} \tag{19}$$

$$\underline{u}^{(1)} = \underline{q}^{(1)} e^{iKt} \tag{20}$$

$\gamma$ is inserted in equation (19) for convenience; $\underline{q}^{(1)}$ is spatial distribution of acoustic velocity, and K is the complex frequency

$$K \equiv \Omega + i\Lambda \tag{21}$$

The amplitudes $p^{(1)}$ and $\underline{q}^{(1)}$ may also be complex.

Thus equation (18) may be written in the form of the nonhomogeneous Helmholtz equation:

$$\nabla^2 p^{(1)} + K^2 p^{(1)} = M_b g^{(1)} \tag{22}$$

where

$$g^{(1)} = iK (\underline{U}\cdot\nabla p^{(1)}) - \nabla\cdot\nabla(\underline{U}\cdot\underline{q}^{(1)}) + \nabla\cdot(\underline{q}^{(1)} \times\underline{\zeta}) \tag{23}$$

$$+ M_b [iK (\underline{q}^{(1)}\cdot\frac{\nabla P}{\gamma} + P\nabla\cdot\underline{q}^{(1)}$$

$$+ \frac{1}{\gamma}\nabla\cdot(P\nabla p^{(1)} + p^{(1)}\nabla P)]$$

The boundary condition on $p^{(1)}$ is found by combining the definition for the admittance function (11) with the momentum equation:

$$\hat{n}\cdot\nabla p^{(1)} = -M_b h^{(1)} \tag{24}$$

where

$$h^{(1)} = -iK A p^{(1)} + \hat{n}\cdot[\nabla\underline{U}\cdot q^{(1)} - \underline{q}^{(1)} \times\underline{\zeta}] \tag{25}$$

$$-\frac{M_b}{\gamma}\hat{n}\cdot[P\nabla p^{(1)} + p^{(1)}\nabla p]$$

and function $h^{(1)}$ is to be evaluated over the chamber bounding surfaces. Equations 22 and 24 constitute a boundary value problem in which solutions of a nonhomegeneous wave equation are sought which satisfy a nonhomogeneous Neumann

boundary condition. It is useful at this point to further expand this set in terms of the mean flow Mach number $M_b$. Note that the eigenvalue K must also be expanded; the goal of the calculation is to find K correct to $O(M_b^2)$ to represent growth rate and frequency shifts due to the high-speed mean flow.

Put

$$
\begin{aligned}
p^{(1)} &= p^{(10)} + M_b\, p^{(11)} + M_b^2\, p^{(12)} + \ldots \\
\underline{q}^{(1)} &= \underline{q}^{(10)} + M_b\, \underline{q}^{(11)} + M_b^2\, \underline{q}^{(12)} + \ldots \\
K &= \Omega^{(10)} + M_b(\Omega^{(11)} + i\Lambda^{(11)}) + M_b^2\, (\Omega^{(12)} + i\Lambda^{(12)}) + \ldots \\
g^{(1)} &= g^{(10)} + M_b\, g^{(11)} + \ldots \\
h^{(1)} &= h^{(10)} + M_b\, h^{(11)} + \ldots
\end{aligned}
\tag{26}
$$

$p^{(10)}$ is the unperturbed mode shape of the acoustic wave; $p^{(11)}$ etc. represent distortions of the waveform caused by the mean flow perturbations. Inserting expansions (26) into the wave equation (22) and boundary condition (24), one finds a series of boundary value problems in increasing orders of $M_b$; the 0 (1) problem obviously corresponds to unperturbed acoustic wave motion in the chamber. Thus

$$\nabla^2 p^{(10)} + \Omega^{(10)^2}\, p^{(10)} = 0 \tag{27}$$

$$\hat{n}\cdot\nabla p^{(10)} = 0 \quad \text{on bounding surfaces} \tag{28}$$

$0\ (M_b)$:

$$\nabla^2 p^{(11)} + \Omega^{(10)^2}\, p^{(11)} = g^{(10)} - 2\Omega^{(10)}\, (\Omega^{(11)} + i\Lambda^{(11)})\, p^{(10)} \tag{29}$$

$$\hat{n}\cdot\nabla p^{(11)} = -h^{(10)} \qquad \text{on bounding surfaces} \tag{30}$$

$O(M_b^2)$:

$$\nabla^2 p^{(12)} + \Omega^{(10)2}\, p^{(12)} = g^{(11)} - [2\Omega^{(10)}\,(\Omega^{(11)} + i\Lambda^{(11)})]\, p^{(11)} \tag{31}$$

$$- [2\Omega^{(10)}\,(\Omega^{(12)} + i\Lambda^{(12)}) + (\Omega^{(11)} + i\Lambda^{(11)})^2]\, p^{(10)}$$

$$\hat{n}\cdot\nabla p^{(12)} = -h^{(11)} \qquad \text{on bounding surfaces} \tag{32}$$

where

$$g^{(10)} = i\Omega^{(10)}\,(\underline{U}\cdot\nabla p^{(10)}) - \frac{i}{\Omega^{(10)}}\nabla\cdot\nabla(\underline{U}\cdot\nabla p^{(10)}) + \frac{i}{\Omega^{(10)}}\nabla\cdot(\nabla p^{(10)} \times \underline{\zeta}) \tag{33}$$

$$h^{(10)} = -i\Omega^{(10)}\,(A^{(r)} + iA^{(i)})\, p^{(10)}$$

$$+ \hat{n}\cdot\left[\frac{i}{\Omega^{(10)}}\,\nabla\underline{U}\cdot\nabla p^{(10)} - \frac{i}{\Omega^{(10)}}\,\nabla p^{(10)} \times \underline{\zeta}\right] \tag{34}$$

$$g^{(11)} = i\Omega^{(10)}\,(\underline{U}\cdot\nabla p^{(11)}) + i(\Omega^{(11)} + i\Lambda^{(11)})\,(\underline{U}\cdot\nabla p^{(10)})$$

$$-\nabla\cdot\nabla\left\{\begin{array}{l}\underline{U}\cdot\left[\dfrac{i}{\Omega^{(10)}}\,\nabla p^{(11)}\,\dfrac{i(\Omega^{(11)} + i\Lambda^{(11)})}{\Omega^{(10)2}}\nabla p^{(10)}\right] \\ \\ -\dfrac{\nabla(\underline{U}\cdot\nabla p^{(10)}}{\Omega^{(10)2}} - (\nabla p^{(10)} \times \underline{\zeta})/\Omega^{(10)2}\end{array}\right\} \tag{35}$$

$$+ \nabla\cdot(q^{(11)} \times \underline{\zeta}) - \frac{\nabla p^{(10)}}{\gamma}\cdot\nabla P$$

$$-P\nabla^2 p^{(10)} + \frac{1}{\gamma}\nabla\cdot\nabla(Pp^{(10)})$$

and

$$h^{(11)} = -i\Omega^{(10)} Ap^{(11)} - i\,(\Omega^{(11)} + i\Lambda^{(11)})Ap^{(10)} \tag{36}$$

$$+ \hat{n} \cdot \left[\overline{\nabla \underline{U} \cdot \underline{q}^{(11)}} - \underline{q}^{(11)} \times \underline{\zeta} - \frac{1}{\gamma} \nabla (P p^{(10)})\right]$$

Previous comments on increasing algebraic complexity with order of expansion are clearly appropriate. Expressions for the velocity amplitude $\underline{q}^{(1)}$ (and its expansion in Mach number $M_b$) are found in terms of pressure fluctuation $p^{(1)}$ by use of the momentum equation. Thus

$$\underline{q}^{(10)} = \frac{i \nabla p^{(10)}}{\Omega^{(10)}}$$

$$\text{and} \quad \underline{q}^{(11)} = \frac{i}{\Omega^{(10)}} \left[\overline{\nabla p}^{(11)} - \frac{(\Omega^{(11)} + i\Lambda^{(11)})}{\Omega^{(10)}} \nabla p^{(10)} + \frac{i}{\Omega^{(10)}} \nabla (\underline{U} \cdot \nabla p^{(10)}) \right.$$

$$\left. + \frac{i}{\Omega^{(10)}} (\nabla p^{(10)} \times \underline{\zeta}) \right] \tag{37}$$

## 2.6. Zeroth-Order Calculations

Equations (27) and (28) represent the classical acoustics of the combustion chamber. Exact solutions can be found for simple chamber geometry; numerical techniques provide information on mode shape $p^{(10)}$ and frequency $\Omega^{(10)}$ for the sometimes complicated configurations used in solid propellant rockets. Since this phase of the problem is thoroughly documented in the literature, no more need be said at this point except that the validity of the higher-order growth rate and frequency calculation obviously depends on having correct estimates for $p^{(10)}$ and $\Omega^{(10)}$ for each chamber mode. The unperturbed frequency is found from the eigenvalue $\Omega^{(10)}$ in dimensional form (cycles/unit time) to be

$$f^{(0)} = \frac{a_o \Omega^{(10)}}{2\pi R} \tag{38}$$

## 2.7. First-Order Calculations

Equations (29) and (30) govern what is commonly referred to as the "linear stability" model of combustion instability. In this calculation, one is seldom interested in the $O(M_b)$ waveform distortion $p^{(11)}$; what is required is an estimate for the growth rate $\Lambda^{(1)}$ and frequency correction $\Omega^{(11)}$. Culick (Ref. 3) derived expressions for these quantities by the Green's function method. A more direct method is to multiply (27) by $p^{(11)}$ and subtract it from (29) multiplied by the unperturbed mode shape $p^{(10)}$. Integrating the result over the chamber volume, employing the divergence theorem and the boundary conditions (28) and (30) yields after a few lines of algebra:

$$(\Omega^{(1)} + i\Lambda^{(1)}) = \frac{1}{2\Omega^{(10)}E^2}\left[\int_V g^{(10)}p^{(10)}dV + \int_S h^{(10)}p^{(10)}dS\right] \tag{39}$$

where $g^{(10)}$ and $h^{(10)}$ are given by equations (33) and (34), and the normalization constant E is found from

$$E^2 = \int_V p^{(10)^2}\, dV \tag{40}$$

Equation (39) can be further simplified (see the papers by Culick for details) by application of vector integral theorems with the results:

$$\Omega^{(11)} = \frac{A^{(i)}}{E^2} \int_S \frac{p^{(10)^2}}{2} \, dS \tag{41}$$

$$\Lambda^{(11)} = - \frac{A^{(r)}}{E^2} \int_S \frac{p^{(10)^2}}{2} \, dS + \frac{1}{E^2} \int_V \underline{u} \cdot \frac{\nabla (p^{(10)})^2}{2} \, dV \tag{42}$$

Growth rate (dimensional) $\alpha$ is found from (42) to be

$$\alpha^{(1)} = - \frac{a_o}{R} M_b \Lambda^{(11)} \quad * \tag{43}$$

where R is the scaling length for the chamber; $a_o$ is the speed of sound. Equation (43) forms the basis for all stability prediction models. The results are discussed at length in the literature (c.f. Refs. 3, 4, 8, 10, etc.) and no more need be said except that, again, it is obvious that higher-order approximations depend on correct estimates for $\Lambda^{(1)}$ and $\Omega^{(1)}$. The 0 ($M_b$) frequency correction $\Omega^{(1)}$ is usually ignored in stability calculations. This is probably due more to lack of information regarding the imaginary part of the admittance than to it being a negligible contribution. The frequency correction in cycles/unit time is found from $\Omega^{(1)}$ to be

$$f^{(1)} = \left(\frac{a_o}{2\pi R}\right) M_b \, \Omega^{(11)} \tag{44}$$

* The superscript is used to emphasize the order of the estimate; higher-order approximations are the goal of this study.

This expression is evaluated in the results section of the report for typical sets of parameters to establish its potential importance.

Another part of the first-order formulation is required before the 0 ($M_b^2$) corrections can be determined. Examination of the $M_b^2$ equation shows that one must know the mode shape correct to 0 ($M_b$) before the higher-order equations can be evaluated. That is the waveform correction $p^{(11)}$ must first be determined. There are two approaches to this problem. One is to seek the eigenfunctions for equation (29) directly. This can be done analytically only for simple geometries. This method is demonstrated in a later section of the report. A more general method is to use a Green's function solution of equation (29) using expansions in terms of the unperturbed eigenfunction (Refs. 3 and 4). This yields an infinite series representation for $p^{(11)}$:

$$p^{(11)} = \sum_{\substack{\beta \\ \beta \neq N}}^{\infty} \frac{p_\beta^{(10)}}{E_\beta^2 \left(\Omega_N^{(10)^2} - \Omega_\beta^{(10)^2}\right)} \left[ \int_V g^{(10)} p_\beta^{(10)} dV + \int_S h^{(10)} p_\beta^{(10)} dS \right] \quad (45)$$

where N refers to the particular mode of oscillation in question; $\beta$ identifies each of the remaining infinity of modal eigenfunctions.* It is the experience of the writer that this is usually a very slowly convergent series. It is possible that direct numerical solutions of equation (29) will be a more efficient technique for determining the mode distortion effects.

## 2.8. Second-Order Corrections

We finally arrive at the target of the present study--to determine the effects of mean flow to 0 ($M_b^2$) on stability and frequency. It is important to note that no influence of mean flow compressibility or variation of mean

* For three dimensional chambers N (and $\beta$) are three-integer sets which identify the mode.

chamber thermodynamic parameters is reflected in the results of the first order calculation; no questions regarding high-speed mean flow effects can be answered by use of Equations (41) and (42). We now calculate $\Omega^{(2)}$ and $\Lambda^{(2)}$ which reflect the effects of interest. Multiplying Equation (27) by $p^{(12)}$ and subtracting (31) multiplied by $p^{(10)}$ yields

$$\Omega^{(12)} + i\Lambda^{(12)} = \frac{1}{2\Omega^{(0)}E^2} \left\{ \begin{array}{l} \int_V g^{(11)}\, p^{(10)}\, dV + \int_S h^{(11)}\, p^{(10)} dS \\ - E^2(\Omega^{(11)} + i\Lambda^{(11)})^2 \\ - 2\Omega^{(10)}(\Omega^{(11)} + i\Lambda^{(11)}) \int_V p^{(10)}\, p^{(11)}\, dV \end{array} \right\} \quad (46)$$

after integration over the chamber volume and application of the boundary conditions. Evaluation of these expressions gives the required information. It is not necessary to determine $p^{(12)}$ explicitly unless even higher order corrections are required.

The application of these results is demonstrated in the following section for a typical motor configuration. It is important to notice that the form of the frequency and growth rate corrections is identical to the first order expression. The significance of this observation is that the very same type of calculation as used in the linear stability model is required to determine the corrections. Once the waveform distortion is known, the rest of the calculation is handled by simply adding correction terms to the integrals already evaluated in the standard codes. The expressions are somewhat more complicated algebraically than their first-order counterparts, but they are easily incorporated by simply adding them to existing codes. In addition to the unperturbed mode shape data utilized in the standard codes, one must provide the following additional input:

1. Waveform distortion $(p^{(11)})$
2. $0\ (M_b^2)$ pressure distribution $(\bar{P})$
3. Reasonable estimate of mean flow velocity distribution $(\underline{U})$

The appendix includes a discussion of methods for estimating the $0(M_b^2)$ compressible pressure distribution and mean flow velocity pattern in a tubular grain.

## 3. APPLICATIONS

The purpose of this section is to demonstrate in detail the application of the theory set forth in the previous parts of the report. A simple motor geometry is analyzed to enable analytic determination of *all* quantities of interest.

The simplest configuration which exhibits the features we desire to emphasize is a tubular grain with high L/D (length-to-diameter) ratio. In what follows, the effects of high-speed, compressible mean flow on the frequency and growth rate of longitudinal waves in such a motor are determined; the results are directly applicable to several tactical rocket designs currently under development. Figure 2 shows the geometry assumed and the coordinate system. The Appendix contains a detailed analysis of the mean flow pattern and thermodynamics appropriate to this configuration.

Assuming longitudinal modes of oscillation ($\beta = \ell = 1, 2, 3...$), solution of the zeroth-order equations yields the familiar results:

$$p^{(10)} = \cos K_\ell Z \tag{47}$$

$$\Omega^{(10)} = K_\ell = \frac{\ell \pi R}{L} \tag{48}$$

where $\ell$ is the mode integer ($\ell = 1$ is the first longitudinal mode, etc.). The unperturbed frequency (from eqn. 38) is

$$f^{(0)} = \frac{\ell a_o}{2L}, \qquad \text{(cycles/unit time)} \tag{50}$$

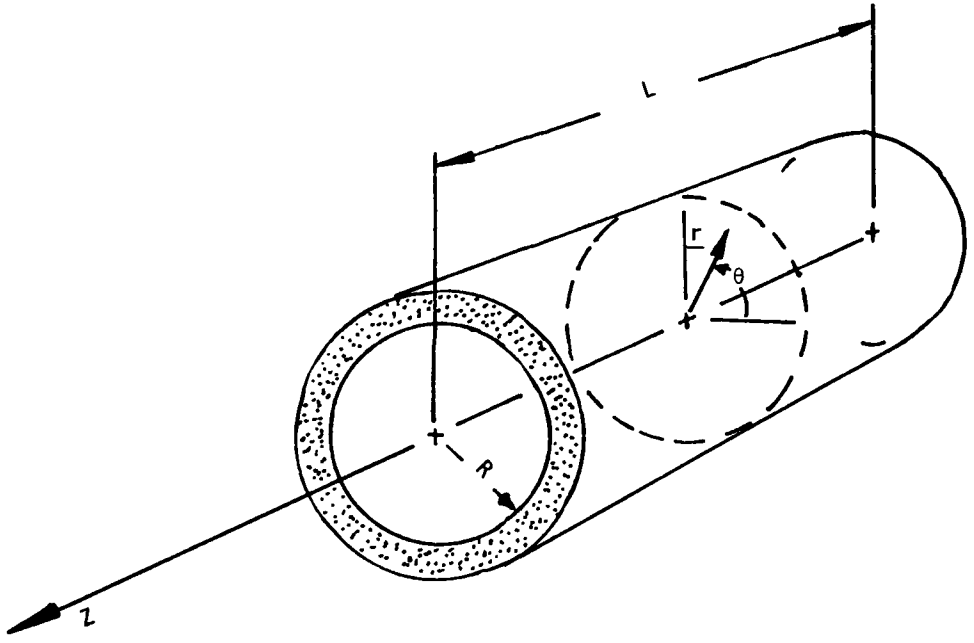


Figure 2. Coordinate System.

a very familiar result. We desire to determine 0 ($M_b^2$) mean flow influences on this frequency and the corresponding growth rate correct to 0 ($M_b^2$).

To apply the linear stability equations (eqn. (41) and (42)) we must first determine the mean flow field correct to 0 ($M_b$). Using the results of the Appendix, one finds that

$$\underline{U} = 2z\,\hat{e}z \tag{51}$$

is a sufficiently accurate statement of the axial velocity component averaged over the chamber cross-section. Since only longitudinal oscillation is assessed, the radial velocity component is immaterial. The corresponding mean field pressure variation is $P = -\frac{\gamma\pi}{2}z^2$. All integrations are easily performed and one finds

$$E^2 = \left(\frac{L\pi}{2R}\right) \tag{52}$$

$$\Omega^{(11)} = A^{(i)} \tag{53}$$

$$\Lambda^{(11)} = 1 - A^{(r)} \tag{54}$$

where an inert surface is assumed at the head-end and the nozzle admittance is ignored to keep this sample calculation as simple as possible. Chamber radius R is used as the scaling length. Application of equations (43) and (44) leads to frequency and growth rate results correct to 0 ($M_b$):

$$f = f^{(0)} + f^{(1)} = \frac{\ell a_o}{2L} \left[ 1 + M_b \left( \frac{A^{(i)}}{\ell \pi} \right) \left( \frac{L}{R} \right) \right] \quad \left( \frac{\text{cycles}}{\text{unit time}} \right) \tag{55}$$

$$\alpha^{(1)} = M_b f^{(0)} \left( \frac{2}{\ell} \right) \left( \frac{L}{R} \right) \left( A^{(r)} - 1 \right) \tag{56}$$

Converting to the more familiar admittance notation we find:

$$\alpha = \frac{4 f^{(0)}}{\ell} \left( \frac{L}{D} \right) \left( A_b^{(r)} - M_b \right) + 0 \left( M_b^2 \right) \tag{57}$$

or

$$\alpha = \frac{4 f^{(0)}}{\ell} \left( \frac{L}{D} \right) \left( R_b - 2M_b \right) + 0 \left( M_b^2 \right) \tag{58}$$

where $R_b = A_b^{(r)} + M_b$ is the response function (Ref. 10). In an actual motor calculation these results would be supplemented by nozzle losses, particulate losses, etc.

To proceed further, it is necessary to determine the waveform distortion by solving equation (29) for $p^{(11)}$. For the cylindrical geometry, the first-order velocity distribution is

$$\underline{q}^{(10)} = - i \sin (k_\ell z)\, \hat{e}_z \tag{59}$$

where $\hat{e}_z$ is the axial unit vector and function $g^{(10)}$ is

$$g^{(10)} = 4ik_\ell \left[\cos (k_\ell z) - k_\ell z \sin (k_\ell z)\right] \tag{60}$$

Thus the differential equation for $p^{(11)}$ reduces to:

$$\frac{d^2 p^{(11)}}{dz^2} + k_\ell^2\, p^{(11)} = -4ik_\ell^2 z \sin (k_\ell z) + \left[4ik_\ell - 2k_\ell (\Omega^{(1)} + \Lambda^{(1)})\right] \cos (k_\ell z) \tag{61}$$

and the boundary conditions (from equation (30)) reduce to:

$$\frac{dp^{(11)}}{dz} = 0 \text{ at } z = 0 \qquad \text{(Head-end)}$$

$$\frac{dp^{(11)}}{dz} = 2i\ell\pi \cos (\ell\pi) \text{ at } z \approx \frac{L}{R} \qquad \text{(Nozzle entrance)} \tag{62}$$

Solutions are found easily by conventional methods and the result is:

$$p^{(1)} = iK_\ell z^2 \cos(k_\ell z) + i(A^{(r)} + iA^{(i)}) \sin(k_\ell z) \qquad (63)$$

Figure 3 shows plots of the waveform $p = p^{(0)} - M_b p^{(1)}$ for the first two longitudinal modes. $A^{(i)}$, the imaginary part of the surface admittance, has only a small effect on the real part of the mode shape. The plots were made with $A^{(i)} = 1$, a typical value, and several values of the real part of the admittance, $A^{(r)}$. The most important feature of the results is the generation of the strong 0 ($M_b$) imaginary part of the mode shape. As will be shown this exerts a strong influence on the chamber frequencies. Note that there is a significant sensitivity of the imaginary mode distortion to the real part of the surface admittance. The range of values of $A^{(r)}$ shown are typical of a variety of propellants.

It is now possible to determine the effects of high-speed mean flow on growth rate and chamber frequency by using equation (46). The velocity waveform distortion from equation (37) is

$$v^{(1)} = \left[ \frac{\sin(k_\ell z)}{k_\ell} - i\left(i(1-A^{(1)}) - \Omega^{(1)}\right) z \cos(k_\ell z) + k_\ell z^2 \sin(k_\ell z) \right] \hat{e}_z \qquad (64)$$

is needed for evaluating the integrals in equation (46).

Function $g^{(II)}$ for the simple geometry assumed is

$$g^{(II)} = - \left[(4+\pi) + iB\right] \cos(k_\ell z) + 4k_\ell^3 z^3 \sin(k_\ell z)$$

$$+ \left[(\pi-10) + 2i\,(5B-C)\right] K_\ell z \sin(k_\ell z) \qquad (65)$$

$$+ \left[4iB - 16 - \pi\frac{(\gamma - 1)}{2}\right] k_\ell^2 z^2 \cos(k_\ell z)$$

where $B = -B^{(II)} + i\,(1 - A^{(II)})$ and $C = C^{(II)} + iA^{(II)}$ are used to simplify the algebra. In terms of the same notation, function $h^{(II)}$ is

$$h^{(II)} = -iC(A^{(r)} + iA^{(i)}) \cos(k_\ell z) - i(A^{(r)} + iA^{(i)})B\, k_\ell z \sin(k_\ell z) \qquad (66)$$

$$- (A^{(r)} + iA^{(i)})\, k_\ell^2 z^2 \cos(k_\ell z)$$

$$+ \frac{n \cdot e_z}{k_\ell} \left\{ \begin{array}{l} 2 \sin(k_\ell z) + \left[(2+\pi) + 4iB\right] K_\ell z \cos(k_\ell z) \\ + \left[6 - \pi/2 - 2iB\right] k_\ell^2 z^2 \sin(k_\ell z) \\ + 2 k_\ell^3 z^3 \cos(k_\ell z) \end{array} \right\} \qquad (67)$$

on boundary surfaces.

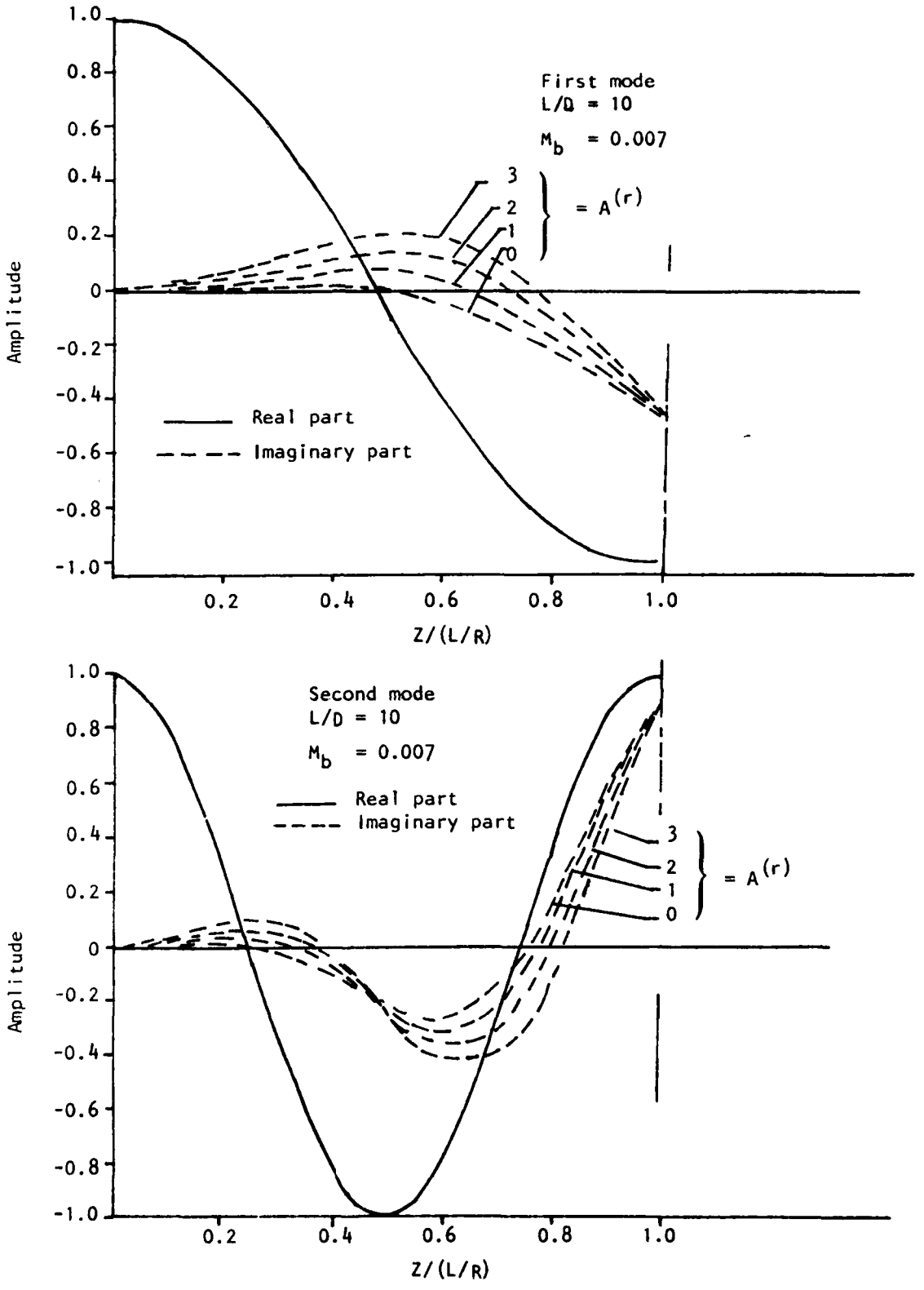


Figure 3. Mode Shapes for the First Two Longitudinal Modes.

The integrals can now be performed and (after some tedious algebra!) one finds

$$A^{(12)} = \left(\frac{L}{D}\right)\left(\frac{4A^{(i)}}{\ell\pi}\right)\left[1 - 2\cos(\ell\pi) - \frac{(\ell\pi)^2}{3} - \frac{A^{(r)}}{2}\right] \tag{68}$$

and

$$B^{(12)} = \left(\frac{L}{D}\right)\left(\frac{2}{\ell\pi}\right)\left\{\begin{array}{l} (\pi+2)\cos\ell\pi - \frac{3}{2} - \frac{\pi}{4}\left(3 + \frac{\gamma-1}{2}\right) \\ \\ + (\ell\pi)^2\left[2\cos(\ell\pi) - \frac{10}{3} - \frac{\pi}{6}\left(\frac{\gamma-1}{2}\right)\right] \\ \\ - \frac{A^{(r)^2}}{2} + 2A^{(r)}\left[1-2\cos(\ell\pi) - \left(\frac{\ell\pi}{3}\right)^2\right] \\ \\ + \frac{A^{(i)^2}}{2} \end{array}\right\} \tag{69}$$

where the previously calculated values of $B^{(10)}$, $B^{(11)}$ and $A^{(11)}$ have been utilized. Presence of damping would thus alter these results, but they are representative of the influence of the high-speed mean flow. Converting to dimensional form, the growth rate and frequency corrections are

$$f^{(2)} = 4f^{(0)} M_b^2 \left(\frac{L}{D}\right)^2 \left(\frac{1}{\ell\pi}\right)^2 \left\{ \begin{array}{l} (\pi + 2)\cos\ell\pi - \frac{3}{2} - \frac{\pi}{4}\left(3 + \frac{\gamma-1}{2}\right) \\ + (\ell\pi)^2 \left[2\cos(\ell\pi) - \frac{10}{3} - \frac{\pi}{6}\left(\frac{\gamma-1}{2}\right)\right] \\ + 2A^{(r)} \left[1 - 2\cos(\ell\pi) - (\ell\pi)^{2/3}\right] \\ + \frac{1}{2}\left(A^{(i)^2} - A^{(r)^2}\right) \end{array} \right\} \quad (70)$$

$$\alpha^{(2)} = 16\pi f^{(0)} M_b^2 \left(\frac{L}{D}\right)^2 \frac{A^{(i)}}{(\ell\pi)^2} \left[2\cos\ell\pi + \frac{(\ell\pi)^2}{3} + \frac{A^{(r)}}{2} - 1\right] \quad (71)$$

Growth rate and frequency are corrected by adding (70) and (71) to (55) and (56) respectively.

Plots of these expressions are displayed in Figures 4 through 8 for first, second and third longitudinal modes. Note that the growth rate correction is linearly dependent on the imaginary part of the wall admittance function $A^{(i)}$. Since $A^{(i)}$ is positive for lower frequencies typical of longitudinal oscillations, this is an additional source of acoustic gain; for higher frequencies, high-speed flow contributes additional damping. The magnitude of the growth rate increment is also dependent on the real part of the admittance as illustrated and is proportional to the square of the port L/D ratio. It is clear that this could be an important growth rate element in motors with high L/D. For instance, in a tactical motor with L/D = 20, $M_b$ = 0.007, $\gamma$ = 1.2, $A^{(r)}$ = 2, $A^{(i)}$ = 2 and f = 300 Hz, the growth rate estimate would be increased by about 45 $sec^{-1}$. As shown in Figures 6 through 8, the frequency shift depends on

$A^{(r)}$ and the square of the motor L/D. A tactical motor with the parameters just mentioned would experience a frequency shift of about -90 Hz (30 percent change) which is clearly significant. Since effects of damping phenomena have not been included in these numerical calculations, the growth rate modification and frequency shifts are most likely not this large in the actual motor.

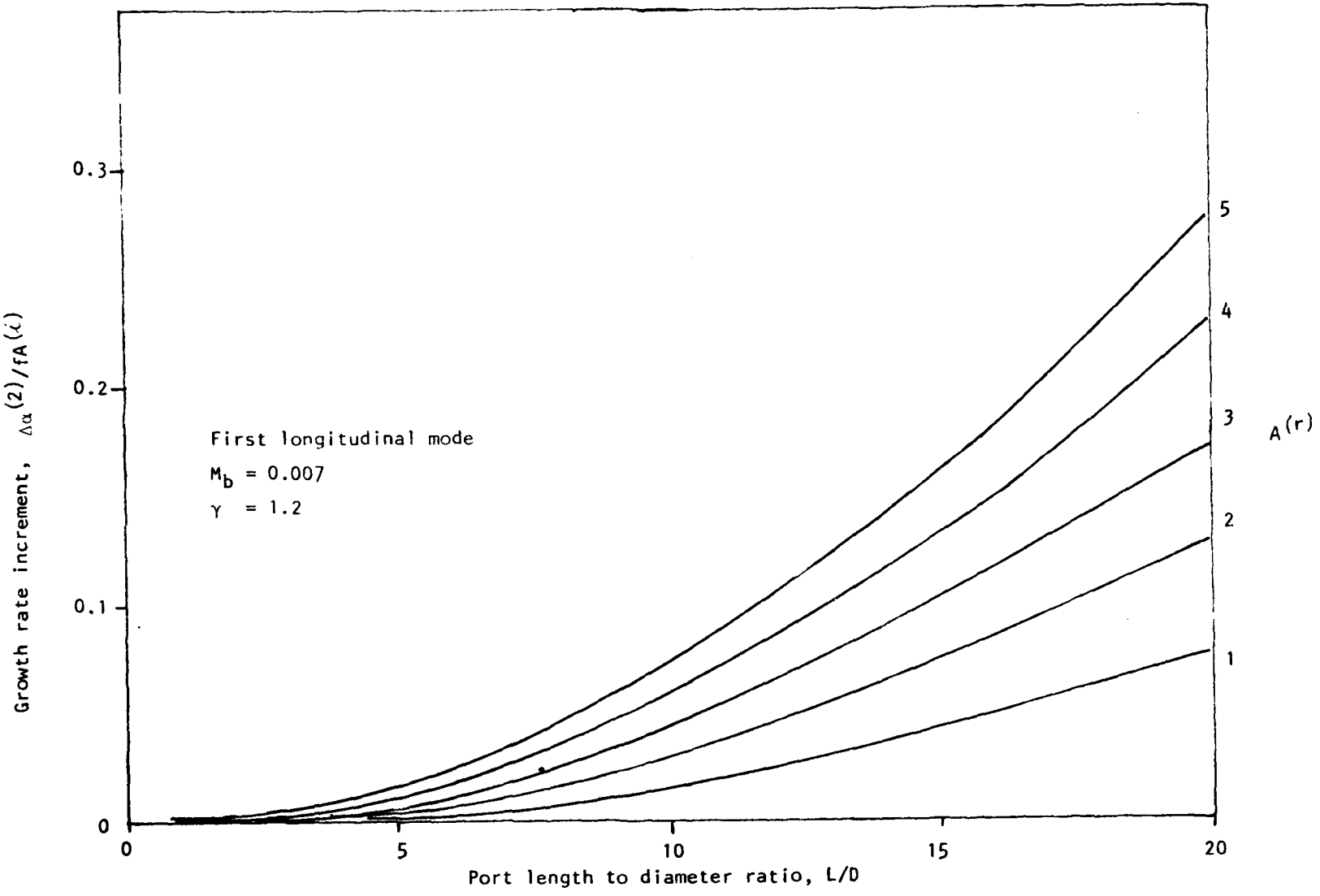


Figure 4. Growth Rate Increment-First Longitudinal Mode.

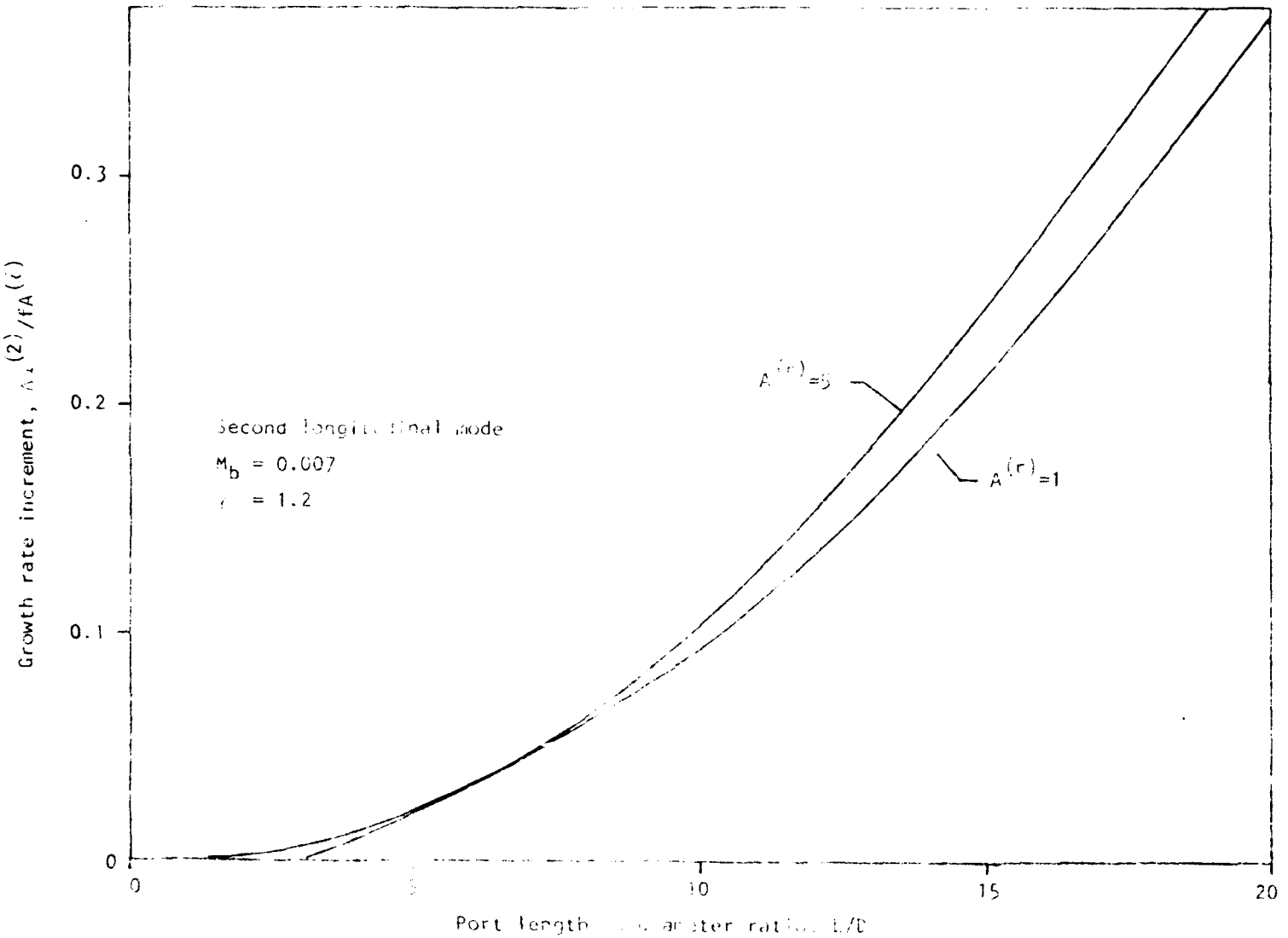


Figure 5. Growth Rate Increment-Second Longitudinal Mode.

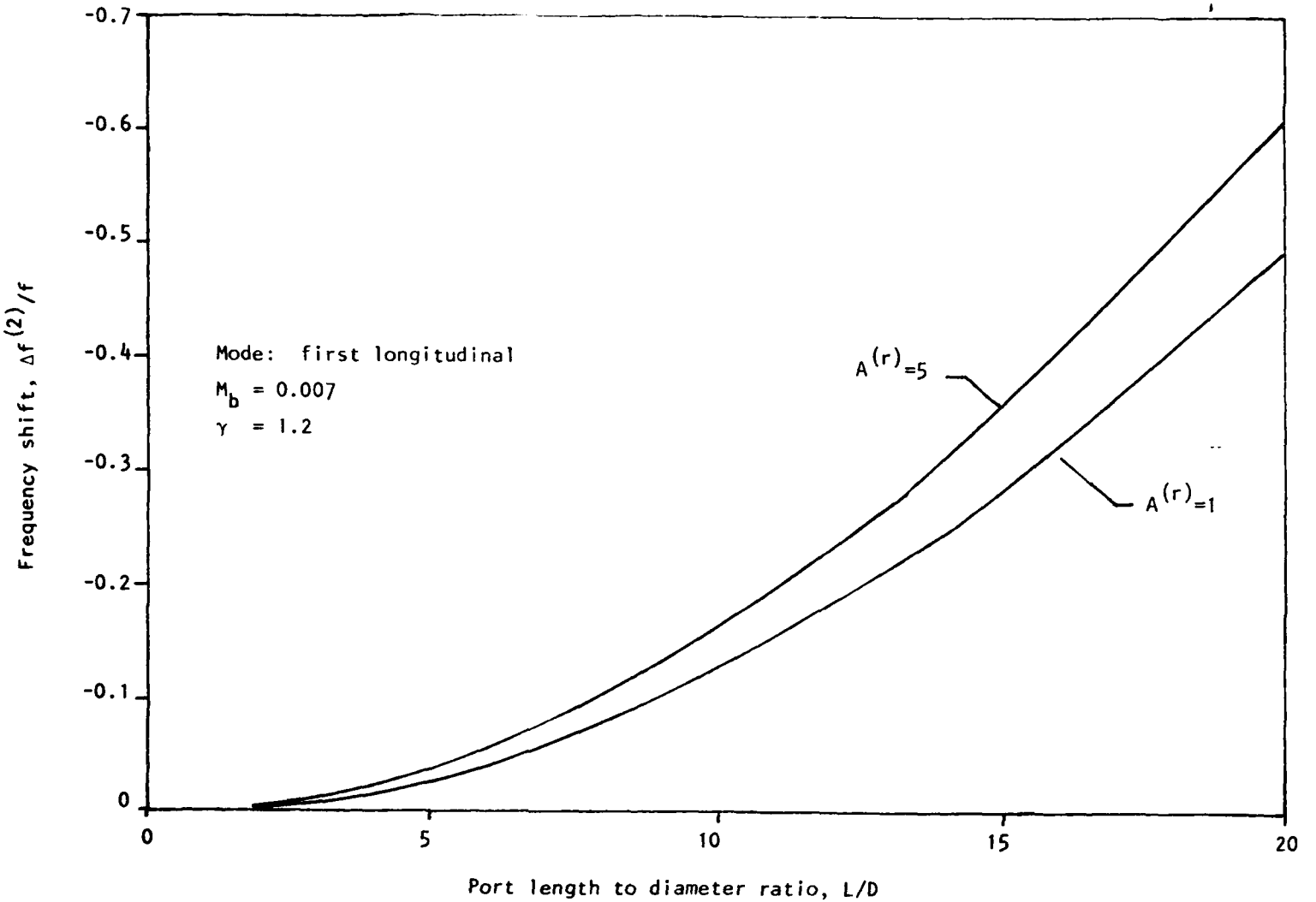


Figure 6. Frequency Shift-First Longitudinal Mode.

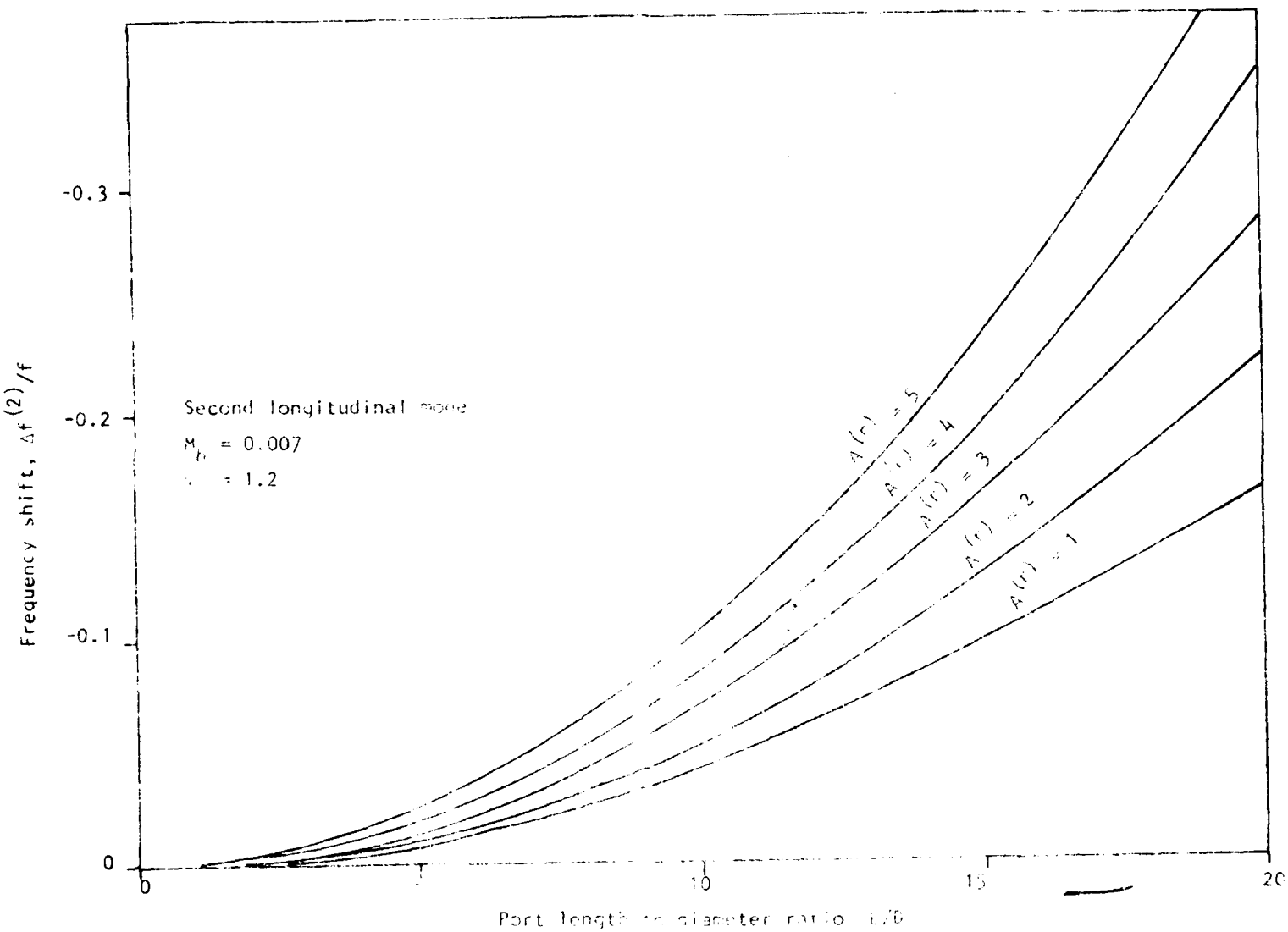


Figure 7. Frequency shift-second longitudinal mode.

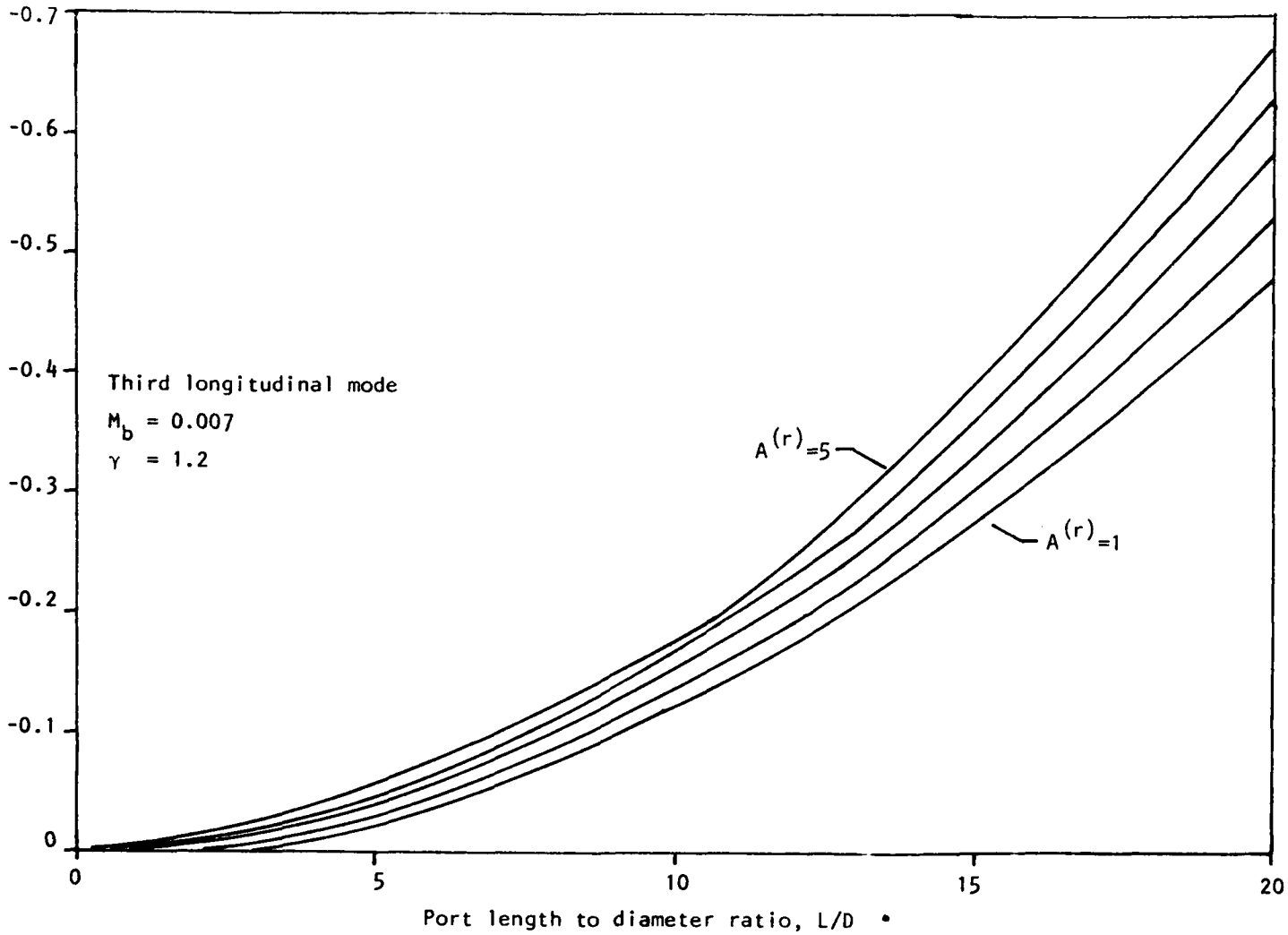


Figure 8. Frequency Shift-Third Longitudinal Mode.

## 4. CONCLUSIONS

The analysis presented in this report demonstrates the importance of several factors which are not included in standard solid propellant rocket combustion stability predictions. The formal linearized model of acoustic instability is based on the assumption that the mean pressure field is uniform and that the flow is incompressible. The present analysis shows that in high L/D rockets or in any motor configuration which exhibit high speed mean flow, the compressibility and mode distortion effects must be accounted for. Frequency shifts of as much as 30 percent of the linear acoustic frequency predictions may be observed in high L/D motors.

It is recommended that corrective terms be added to standard stability codes to incorporate the mean flow terms discussed. It will be necessary to provide means of calculating the mode shape distortion correct to $O(M_0^2)$. This will most easily be accomplished by numerical methods. It is suggested that analytical solutions (similar to the one presented here for longitudinal modes in a tubular grain) be carried out for other [illegible]. These analytical solutions might include: 1) tangential modes in high L/D tubular grain, 2) high speed slot flow, and 3) high speed flow across submerged nozzles. Such results would prove useful in checking computer codes developed later for the more general problem.

## REFERENCES


1. Bird, J. T., McClure, F. T., and Hart, R. W., "Acoustic Instability in the Transverse Modes of Solid Propellant Rockets," 12th International Astronautical Congress, Academic Press, 1963.

2. Cantrell, R. H., and Hart, R. W., "Interaction Between Sound and Flow in Acoustic Cavities: Mass, Momentum, and Energy Considerations," Journal of the Acoustical Society of America, Vol. 36, No. 4, April 1964.

3. Culick, F. E. C.,"Acoustic Oscillations in Solid Propellant Rocket Chambers," Astronautica Acta, Vol. 12, No. 2, 1966.

4. Culick, F. E. C., "Interactions Between the Flow Field, Combustion, and Wave Motions in Rocket Motors," NWC-TP-5349, Naval Weapons Center, China Lake, CA, June 1972.

5. Cole, J. D., and Kevorkian, J., "Uniformly Valid Asymptotic Approximations for Certain Nonlinear Differential Equations." Nonlinear Differential Equations and Nonlinear Mechanics, Academic Press, 1963.

6. Nayfeh, A. H., Perturbation Methods, Wiley, 1973.

7. Flandro, G. A.,"Solid Propellant Admittance Corrections," Journal of Sound and Vibration, Vol. 36, No. 3, 1974.

8. Culick, F. E. C.,"Rotational Axisymmetric Mean Flow and Damping of Acoustic Waves in a Solid Propellant Rocket," AIAA Journal, Vol. 4, No. 8, August 1966.

9. Flandro, G. A., "Rotating Flows in Acoustically Unstable Rocket Motors," PhD Thesis, California Institute of Technology, 1967.

10. Anonymous, T-BURNER MANUAL, CPIA Publication No. 191, November 1969.

11. Culick, F. E. C., "Rotational Axisymmetric Mean Flow and Damping of Acoustic Waves in a Solid Propellant Rocket," AIAA Journal, Vol. 4, No. 8, August 1966, pp. 1462-1464.

12. Dunlap, R., et. al., "Flowfield in the Combustion Chamber of a Solid Propellant Rocket Motor," AIAA Journal, Vol. 12, No. 10, October 1974, pp. 1440-1442.

13. Beddini, R. A., "A Reacting Turbulent Boundary Layer Approach to Solid Propellant Erosive Burning," AFOSR-TR-77-1310, November 1977.

14. Beddini, R. A., "On the Scaling of Solid Propellant Erosive Burning: The Threshold Condition," Proceedings of the 15th JANNAF Combustion Meeting, Newport, R.I., September 1978.

15. Huesmann, K., and Echert, E. R. G., "Untersuchungen über die Laminare Strömung und den Umschlag zur Turbulenz in Porösen Rohren mit gleichmässiger Einblasung durch die Rohrwand," Wörme und Stoffübertragung, Bd. 1, 1968, s. 2.

## APPENDIX

## COMPRESSIBLE, ROTATIONAL AXISYMMETRIC FLOW IN A SOLID PROPELLANT ROCKET

### 1. INTRODUCTION

Required for the assessment of high-speed flow effects in acoustic combustion instability is a practical and realistic model of the compressible mean flow in the combustion chamber. Such a model would also be of obvious utility in studies of erosive burning, growth of metallic oxide particles and velocity coupling effects. Results from detailed computer models of the chamber flow are usually not in a form useful in theoretical investigations; one-dimensional models do not represent the geometrical flow features which are crucial in the problems mentioned.

The incompressible axisymmetric solution for steady rotational flow in a cylindrical rocket grain devised by Culick (Ref. 11) is the starting point for the present investigation. It was shown by Dunlap et. al. (Ref. 12) that the Culick model closely satisfies the viscous equations of motion, and the results were experimentally verified using a cold flow apparatus. In what follows, Culick's solution is generalized to include the effects of compressibility in the mean flow field. The results of the extended analysis are verified by comparison to a one-dimensional numerical solution. An important feature of the model is its simplicity; this greatly enhances its value in theoretical studies of the type described above.



### 2. ANALYSIS

The steady, compressible, rotational axially symmetric flow of a perfect gas is governed by

$$\frac{\partial^2\psi}{\partial r^2} - \frac{1}{r}\frac{\partial\psi}{\partial r} + \frac{\partial^2\psi}{\partial z^2} = \frac{\nabla\rho}{\rho}\cdot\nabla\psi - r\rho\zeta \qquad \text{(A1)}$$

11. Culick, F. E. C., "Rotational Axisymmetric Mean Flow and Damping of Acoustic Waves in a Solid Propellant Rocket," AIAA Journal, Vol. 4, No. 8, August 1966, pp. 1462-1464.

12. Dunlap, R., et. al., "Flowfield in the Combustion Chamber of a Solid Propellant Rocket Motor," AIAA Journal, Vol. 12, No. 10, Oct. 1974, pp. 1440-1442.

$$\rho\nabla\left[\frac{\nabla\psi.\nabla\psi}{2\,(r\rho)^2}\right] + \zeta\,\frac{\nabla\psi}{r} = -\,\frac{\nabla P}{\gamma} \qquad (A2)$$

$$P = \rho^{\gamma} \qquad (A3)$$

where the continuity equation has been exactly satisfied by specification of the stream function $\psi$ such that

$$u = -\left(\frac{1}{r\rho}\right)\frac{\partial\psi}{\partial z} \qquad (A4)$$

$$w = \left(\frac{1}{r\rho}\right)\frac{\partial\psi}{\partial r} \qquad (A5)$$

u and w are the radial and axial velocity components respectively. Equation A1 is the vorticity equation; $\zeta$ is the azimuthal component of vorticity. Radial and axial vorticity components are zero in axisymmetric flow. Equation A2 is the momentum equation and Equation A3 is the energy/state relationship. Viscous force terms do not appear explicitly in the momentum equation because the appropriate length scale is the chamber radius. This makes the viscous force much smaller than momentum and pressure effects; no boundary layer of the classical type is formed and vorticity fills the entire flow field. All flow properties are made dimensionless in terms of the stagnation thermodynamic properties $a_o$, Po and $\rho o$ at the head-end of the chamber; chamber radius R is the characteristic length. Boundary conditions are

$$\begin{aligned} u = w &= o && \text{at } r = z = o \\ u &= -M_b && \text{at } r = 1 \\ w &= 0 && \text{at } r = 1 \end{aligned} \qquad (A6)$$

The latter constraint requires the flow to satisfy the no slip condition at the burning surface; this introduces vorticity into the flow and also forces it to behave as a viscous fluid[2].

The problem is readily solved by standard perturbation techniques; the mean flow Mach number $M_b$ at the burning surface is the appropriate small parameter. The expansions are

$$\psi = M_b \psi^{(o)} + M_b^3 \psi^{(1)} + \ldots$$

$$\rho = 1 + M_b^2 \rho^{(1)} + \ldots$$

$$P = 1 + M_b^2 P^{(1)} + \ldots$$

$$\zeta = M_b \zeta^{(o)} + M_b^3 \zeta^{(1)} + \ldots \qquad \text{(A7)}$$

The first order solution is governed by

$$\frac{\partial^2 \psi^{(o)}}{\partial r^2} - \frac{1}{r}\frac{\partial \psi^{(o)}}{\partial r} + \frac{\partial^2 \psi^{(o)}}{\partial z^2} = -\pi^2 r^2 \psi^{(o)} \qquad \text{(A8)}$$

where $\zeta^{(o)} = \pi^2 r \psi^{(o)}$ to satisfy the boundary conditions specified. This differs from the vorticity used by Culick (Ref. 11) by an additional factor of $\pi$. The solution to Equation A8 is

$$\psi^{(o)} = z \sin\left(\frac{\pi r^2}{2}\right) \qquad \text{(A9)}$$

and the corresponding velocity components are

$$u^{(o)} = -\frac{1}{r}\sin\left(\frac{\pi r^2}{2}\right)$$

$$w^{(o)} = \pi z \cos\left(\frac{\pi r^2}{2}\right) \tag{A10}$$

Note that the next terms in the expansion for $\psi$ are $0\ (M_b{}^3)$ so that Equation A10 represents the velocity field to a high degree of precision.

Equation A2 is now expanded to yield information regarding the thermodynamic properties of the flow field.

Retaining terms of $0\ (M_b{}^2)$, one finds

$$-\frac{\nabla P^{(1)}}{\gamma} = \pi^2 \psi^{(o)}\ \nabla\psi^{(o)} + \nabla\left[\frac{\nabla\psi^{(o)} \cdot \nabla\psi^{(o)}}{2r^2}\right] \tag{A11}$$

Noting that $\psi^{(o)}\ \nabla\psi^{(o)} = \nabla\frac{\psi^{(o)2}}{2}$, equation A11 can be integrated directly with the result

$$p^{(1)} = -\frac{\gamma}{2}\left[\pi^2\ \psi^{(o)2} + \frac{\nabla\psi^{(o)} \cdot \nabla\psi^{(o)}}{r^2}\right] \tag{A12}$$

The constant of integration is zero to satisfy stagnation requirements at the head-end. Inserting Equation A9 yields

$$p^{(1)} = -\frac{\gamma}{2}\left[\pi^2 z^2 + \frac{\sin^2\left(\frac{\pi r^2}{2}\right)}{r^2}\right] \tag{A13}$$

and using Equation A13 in an expansion of Equation A3 gives

$$\rho^{(1)} = -\frac{1}{2}\left[\pi^2 z^2 + \frac{\sin^2\left(\frac{\pi r^2}{2}\right)}{r^2}\right] \tag{A14}$$

These functions represent models of the compressible thermodynamic properties correct to $0\ (M_b{}^4)$.

3. RESULTS

The analysis yields a simple and practical representation for the flow field in a tubular rocket grain.

Rewriting the equations in terms of physical variables,

$$\bar{u} = v_b\left[-\left(\frac{R}{r}\right)\sin\left(\frac{\pi r^2}{2R^2}\right)\hat{e}_r + \left(\frac{\pi z}{R}\right)\cos\left(\frac{\pi r^2}{2R^2}\right)\hat{e}_z\right] + 0(M_b{}^3)$$

$$P = Po\left\{1 - \frac{\gamma}{2}\left(\frac{v_b}{a_o}\right)^2\left[\left(\frac{\pi z}{R}\right)^2 + \left(\frac{R}{r}\right)^2 \sin^2\left(\frac{\pi r^2}{2R^2}\right)\right]\right\} + 0(M_b{}^4)$$

$$\rho = \rho o\left\{1 - \frac{1}{2}\left(\frac{v_b}{a_o}\right)^2\left[\left(\frac{\pi z}{R}\right)^2 + \left(\frac{R}{r}\right)^2 \sin^2\left(\frac{\pi r^2}{2R^2}\right)\right]\right\} + 0(M_b{}^4)$$

$$T = To\left\{1 - \left(\frac{\gamma-1}{2}\right)\left(\frac{v_b}{a_o}\right)^2\left[\left(\frac{\pi z}{R}\right)^2 + \left(\frac{R}{r}\right)^2 \sin^2\left(\frac{\pi r^2}{2R^2}\right)\right]\right\} + 0(M_b{}^4) \tag{A15}$$

where $v_b = \rho_p \dot{r}/\rho_o = a_o M_b$ is the velocity at the chamber boundary due to efflux of combustion gases. r and z are the radial and axial position c coordinates and R is the chamber radius.

Figure A1 shows the streamline pattern corresponding to the above solution.

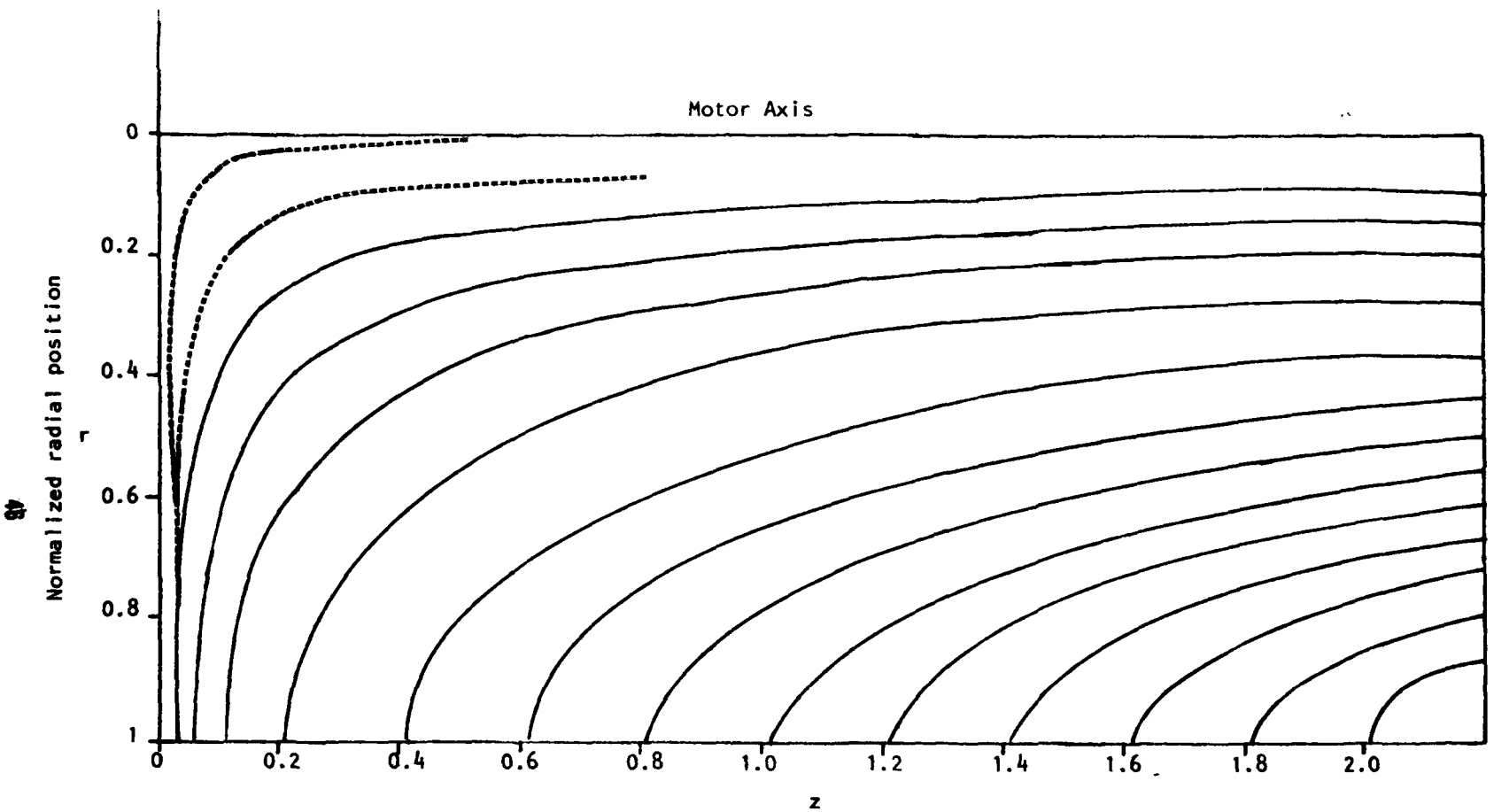


Figure A1. Streamline Pattern

Figure A2 illustrates the velocity profiles. The upper plot shows the axial velocity distribution; the lower shows the radial velocity profile. The axial velocity is conveniently referenced to the centerline speed

$$V_c = \frac{\pi v_b z}{R} \tag{A16}$$

while the appropriate reference speed for the radial component is the efflux velocity $v_b$.

Figure A3 shows the pressure variation along the motor axis. It is apparent from Equations A15 that the pressure varies quadratically with axial position. At the centerline, the variation is given by

$$\frac{Pc-Po}{\left(\frac{\gamma PoM_b^2}{2}\right)} = -\left(\frac{\pi z}{R}\right)^2 \tag{A17}$$

where the pressure scale is the reference dynamic pressure based on chamber pressure at the head-end and the burning surface Mach number $M_b$. A typical value for $\gamma PoM_b^2/2$ is 0.02 (corresponding to $Po \approx 600$ lb/in$^2$ and $M_b = 0.007$). At the burning surface, the pressure variation is

$$\Delta P_b = \frac{Pb-Po}{\left(\frac{\gamma PoM_b^2}{2}\right)} = -\left[\left(\frac{\pi z}{R}\right)^2 + 1\right] \tag{A18}$$

Thus the radial pressure gradient is much smaller than the axial component.

Since the flow field predictions based on the present analysis are not valid when sonic speed is reached, it is necessary to calculate the limiting axial position. It is readily shown that a Mach number of unity is exceeded if z/R exceeds the critical value

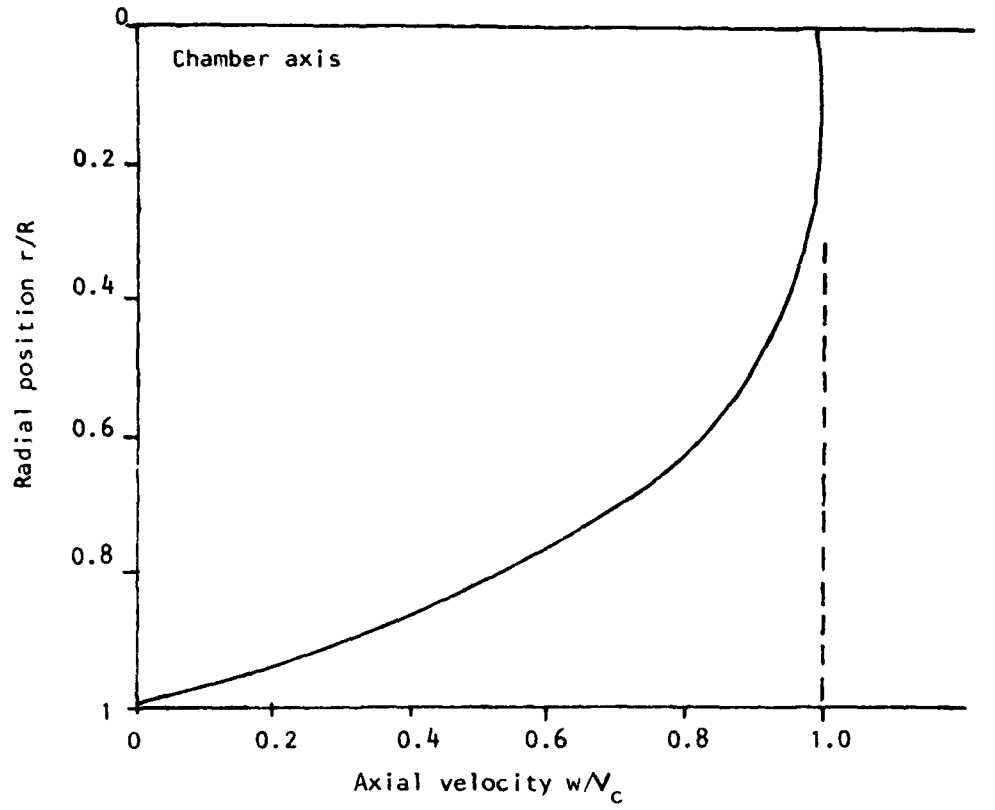


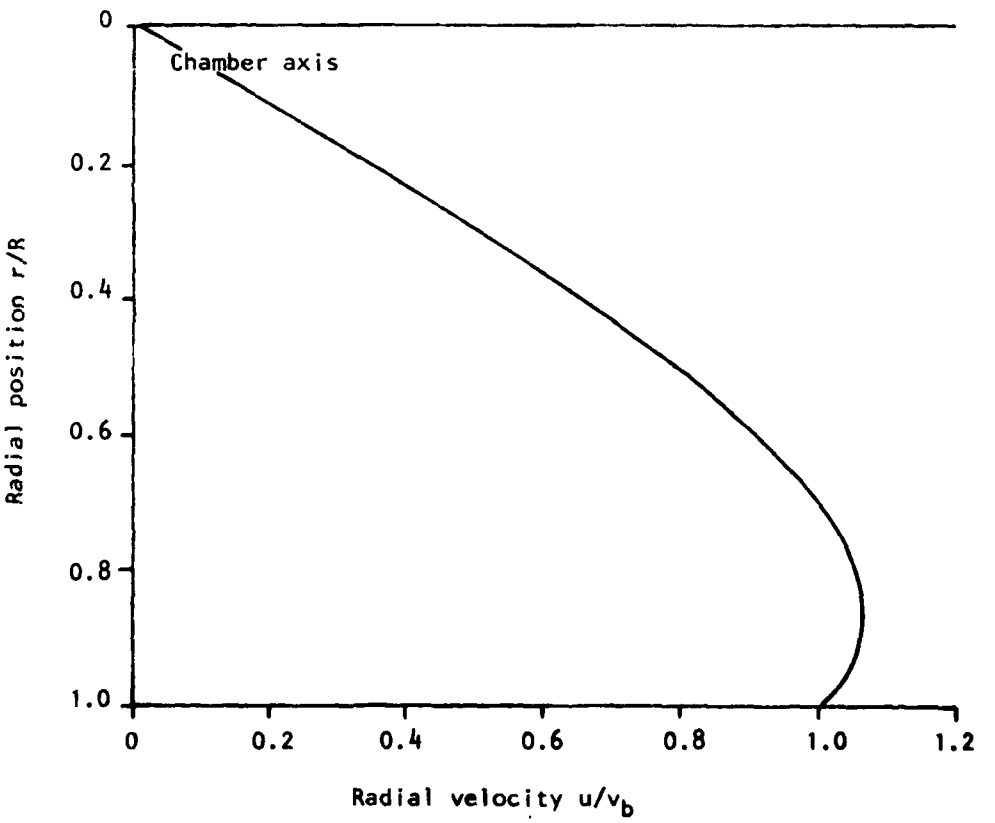


Figure A2. Velocity Profiles.

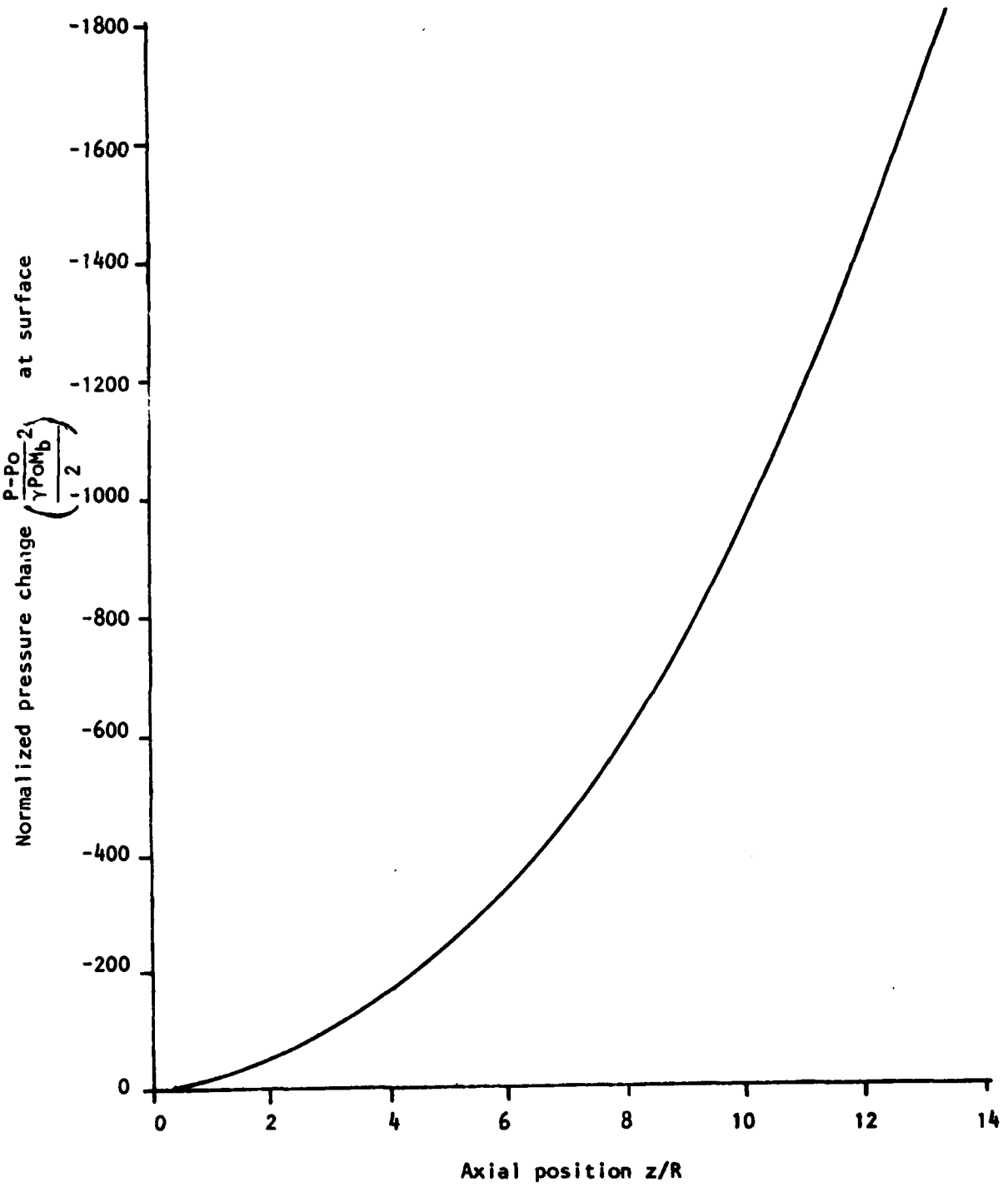


Figure A3. Pressure Variation Along Motor Axis.

$$\left(\frac{z}{R}\right)_{max} = \frac{\sqrt{2/(\gamma+1)}}{\pi M_b} \tag{A19}$$

where $M_b$ is the burning surface Mach number and $\gamma$ is the ratio of specific heats. For example, if $\gamma = 1.2$, $M_b = 0.007$, $(z/R)_{max} = 43.4$.
Thus for these typical conditions, sonic flow is reached if the motor L/D exceeds about 22.

## 4. HIGHER-ORDER CORRECTIONS

The results presented above suggest that a continuation of the perturbation solution can yield a more accurate representation of the flow field. Some initial attempts in this direction are presented in this section. It should be emphasized that the impact of the initial assumptions is likely to be of crucial importance in determining the validity of the higher-order correction terms. In particular, neglect of viscous terms and the influence of turbulence and the turbulent transition process in the formulation may make such efforts of academic interest only. It is the opinion of the writer that attempts to produce a theory for motors with large L/D should incorporate a turbulent flow model in a rational way. Methods analogous to development of turbulent pipe flow might be appropriate. Considerable numerical work has been accomplished in this area, notably the work of Beddini (Refs. 13 and 14), which indicates the importance of viscous elements of the flow field. Other experimental studies (Ref. 15) also suggest a similar conclusion, although some features of the test procedure and their influence on turbulent properties of the flow are in question. It is quite likely that the most desirable feature of the present analysis - its simplicity - will most certainly be lost if viscous effects, especially turbulence, are explicitly included. In spite of these considerations, the attempt is made in what follows to extend the inviscid model to $O(M_b^4)$. It will be shown that the corrections are apparently only important for large length to diameter ratio combustion chambers.


13. Beddini, R. A., "A Reacting Turbulent Boundary Layer Approach to Solid Propellant Erosive Burning," AFOSR-TR-77-1310, November 1977.

14. Beddini, R. A., "On the Scaling of Solid Propellant Erosive Burning: The Threshold Condition," Proceedings of the 15th JANNAF Combustion Meeting, Newport, R.I., September 1978.

15. Huesmann, K., and Echert, E. R. G., "Untersuchungen über die Laminare Stromung und den Umschlag zur Turbulenz in Porösen Rohren mit gleichmässiger Einblasung durch die Rohrwand," Wörme und Stoffübertragung, Bd. 1, 1968, s. 2.

The stream function to $O(M_b^3)$ is governed by

$$\frac{\partial^2\psi^{(1)}}{\partial r^2} - \frac{1}{r}\frac{\partial\psi^{(1)}}{\partial r} + \frac{\partial^2\psi^{(1)}}{\partial z^2} = \nabla\rho^{(1)} \cdot \nabla\Psi^{(0)} - r\rho^{(1)}\rho^{(0)} - r\rho^{(1)} \tag{A20}$$

and the momentum balance to $O(M_b^4)$ requires that

$$\rho^{(1)}\nabla\left[\frac{\nabla\Psi^{(0)}\cdot\nabla\Psi^{(0)}}{2r^2}\right] + \nabla\left[\frac{\nabla\Psi^{(0)}\cdot\nabla\Psi^{(1)} - \rho^{(1)}\nabla\Psi^{(0)}\cdot\nabla\Psi^{(0)}}{r^2}\right] \tag{A21}$$

$$+ \frac{1}{r}\left[\rho^{(0)}\nabla\Psi^{(1)} + \rho^{(1)}\nabla\Psi^{(0)}\right] = -\frac{\nabla P^{(2)}}{\gamma}$$

where $\rho^{(0)} = \pi^2 r\Psi^{(0)}$ and $\rho^{(0)}$ and $\Psi^{(0)}$ are given by Equations A9 and A14 as before. The boundary conditions are

$$\frac{\partial\psi^{(1)}}{\partial r} = \rho^{(1)}\frac{\partial\psi^{(0)}}{\partial r} \qquad \text{at } z = 0 \text{ or } r = 1 \tag{A22}$$

and

$$\frac{\partial\psi^{(1)}}{\partial z} = \rho^{(1)}\frac{\partial\psi^{(0)}}{\partial z} \qquad \text{at } z = 0 \text{ and } r = 0 \text{ or } r = 1 \tag{A23}$$

A solution which satisfies these requirements is

$$\psi^{(1)} = -\frac{\sin(\frac{\pi r^2}{2})}{2}\left[\frac{\pi^2 z^2}{3} + 1\right] z \tag{A24}$$

The corresponding velocity components are

$$u^{(1)} = \frac{\sin(\frac{\pi r^2}{2})}{2r}\left[1 - \frac{\sin^2(\frac{\pi r^2}{2})}{r^2}\right] \tag{A25}$$

and

$$w^{(1)} = \pi z \cos(\frac{\pi r^2}{2})\left[\frac{\pi^2 z^2}{3} + \frac{\sin^2(\frac{\pi r^2}{2})}{2r^2} - \frac{1}{2}\right] \tag{A26}$$

Thus the velocity field is determined to $O(M_b^3)$. Notice that only the axial correction is likely to be of any consequence; in fact, an appropriate approximation is

$$w^{(1)} \approx \frac{\pi^3 z^3}{3}\cos(\frac{\pi r^2}{2}) \tag{A27}$$

since the other terms are of order $zM_b^3$ or smaller. Thus the corrected centerline pressure distribution is to good approximation:

$$P = Po - \frac{\gamma PoM_b^2}{2} \left(\frac{\pi z}{R}\right)^2 \left[1 + \frac{M_b^2}{3} \left(\frac{\pi z}{R}\right)^2 + O(M_b^4)\right] \tag{A28}$$

in physical variables. For typical chamber parameters, the correction is of the order of 23 percent for $\left(\frac{z}{R}\right) = 40$.

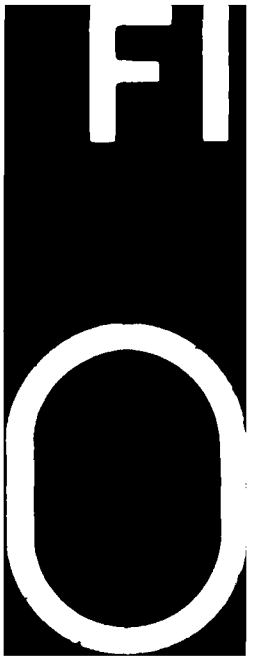
FI